Lawrence Berkeley National Laboratory

Title
CONTROL OF RESPIRABLE PARTICLES AND RADON PROGENY WITH PORTABLE AIR CLEANERS

Permalink
https://escholarship.org/uc/item/4xn922bc

Author
Offermann, F.J.

Publication Date
1984-02-01

Lawrence Berkeley Laboratory
UNIVERSITY OF CALIFORNIA

APPLIED SCIENCE
DIVISION
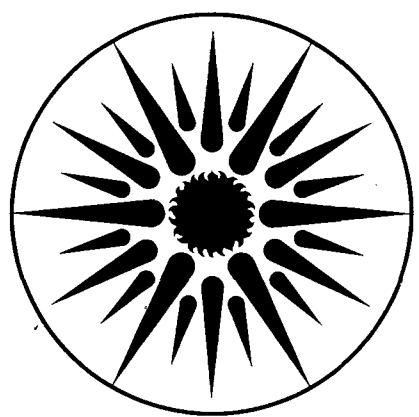
CONTROL OF RESPIRABLE PARTICLES AND RADON PROGENY
WITH PORTABLE AIR CLEANERS

F.J. Offermann, R.G. Sextro, W.J. Fisk,
W.W. Nazaroff, A.V. Nero, K.L. Revzan,
and J. Yater

February 1984

**APPLIED SCIENCE
DIVISION**

DISCLAIMER

This document was prepared as an account of work sponsored by the United States Government. While this document is believed to contain correct information, neither the United States Government nor any agency thereof, nor the Regents of the University of California, nor any of their employees, makes any warranty, express or implied, or assumes any legal responsibility for the accuracy, completeness, or usefulness of any information, apparatus, product, or process disclosed, or represents that its use would not infringe privately owned rights. Reference herein to any specific commercial product, process, or service by its trade name, trademark, manufacturer, or otherwise, does not necessarily constitute or imply its endorsement, recommendation, or favoring by the United States Government or any agency thereof, or the Regents of the University of California. The views and opinions of authors expressed herein do not necessarily state or reflect those of the United States Government or any agency thereof or the Regents of the University of California.

CONTROL OF RESPIRABLE PARTICLES AND RADON PROGENY
WITH PORTABLE AIR CLEANERS

Francis J. Offermann, Richard G. Sextro,
William J. Fisk, William W. Nazaroff, Anthony V. Nero,
Kenneth L. Revzan, and Jane Yater

Building Ventilation and Indoor Air Quality Program
Lawrence Berkeley Laboratory
University of California
Berkeley, California 94720

ABSTRACT

Eleven portable air cleaning devices have been evaluated for control of indoor concentrations of respirable particles and radon progeny. Following injection of cigarette smoke and radon in a room-size chamber, decay rates for particles and radon progeny concentrations were measured with and without air cleaner operation. Particle concentrations were obtained for total number concentration and for number concentration by particle size. In tests with no air cleaner the natural decay rate for cigarette smoke was observed to be 0.2 hr^{-1}. Air cleaning rates for particles were found to be negligible for several small panel-filters, a residential ion-generator, and a pair of mixing fans. The electrostatic precipitators and extended surface filters tested had significant particle removal rates, and a HEPA-type filter was the most efficient air cleaner. The evaluation of radon progeny control produced similar results; the air cleaners which were effective in removing particles were also effective in removing radon progeny. At low particle concentrations plateout of the unattached radon progeny is an important removal mechanism. Based on data from these tests, the plateout rate for unattached progeny was found to be 15 hr^{-1}. The unattached fraction and the overall removal rate due to deposition of attached and unattached nuclides have been estimated for each radon decay product as a function of particle concentration. While air cleaning can be effective in reducing total radon progeny, concentrations of unattached radon progeny can increase with increasing air cleaning.

keywords: air cleaning, ion-generator, instrumentation deposition, electrostatic filtration, indoor air quality, mechanical filtration, plateout, radon, radon progeny, residential buildings, respirable particles, tobacco smoke, unattached fraction, working level ratio.

TABLE OF CONTENTS

I. INTRODUCTION

As residential ventilation rates are reduced through weatherization measures or new construction practices, indoor pollutant concentrations may increase. One strategy for controlling indoor air contaminants in residences that is receiving increased consideration is air cleaning, especially for particulate phase contaminants. Air cleaners for particulate control are available as both in-duct devices, which are designed to be integrated with a forced-air heating/cooling system, and as unducted devices which are portable and designed primarily for cleaning the air in one room. In the past few years a variety of portable residential air cleaners have appeared on the market. Aggressive national advertising along with an increased consumer awareness of indoor air pollution has resulted in the rapid formation of a $150 million/year market (ACHR, 1982) embracing approximately 50 manufacturers. Prices range from $10 to $450 with the majority of the sales going to manufacturers of the less expensive fan-filter units ($10-40). Because there is currently no standard testing procedure, little information regarding the performance of these air cleaners beyond the general claims of the manufacturers is available to consumers. The results of the few tests that have been done with these devices (Whitby 1983, New Shelter, 1982) indicate a wide range in performance.

In this paper we describe the types of devices available for removing respirable particles from the air, discuss our *in situ* measurement technique, and report the results from tests of ten different models of air cleaners. The impact of air cleaning on particulate concentrations and on the concentrations and attached fractions of radon progeny are discussed.

Indoor Particles

There exists a wide variety of particle sources in the indoor environment as listed in Table 1. Indoor sources of combustion-generated particles include tobacco smoking, use of unvented combustion appliances (e.g. gas range and kerosene heaters), wood stoves or fireplaces. Other sources include infiltration of outdoor particles, use of aerosol sprays, and the wear and sloughing of building materials. Particles can exist in either solid or liquid phase or in a combination.

The shape of solid particles can be fibrous, spherical, or irregular, while liquid particles are usually spherical.

The health effects resulting from inhaling particles depend on both the chemical composition of the particles and the site at which they deposit within the respiratory system. Particles deposited in the upper portion of the respiratory system are continuously cleared away by a ciliated mucous lining. Adverse health effects are typically associated with particle deposition deep in the unciliated tracheobronchial or alveolar regions of the lung. The probability of a particle being deposited in a specific region of the lung is mainly a function of the aerodynamic diameter of the particle. Figure 1 depicts the fraction of particles deposited in different regions of the lung as a function of the particle size (Task Group on Lung Dynamics, 1966). From this figure it can be seen that only small particles, less than 3.0 μm in diameter, have a high probability of being deposited in the pulmonary regions of the lung, while larger particles are removed in the protected upper portion of the respiratory system. Particles deposited in the pulmonary region have long residence times, providing an opportunity for the tissues in contact to absorb any harmful substances. The deposition and concentration of toxic substances onto a small area of lung tissue increases the probability for local damage or absorption into the blood stream.

Particules may be intrinsically toxic due to their chemical or physical characteristics (e.g. lead, asbestos) or they may act as a carrier of an adsorbed toxic substance (e.g. BaP, HCHO, radon progeny). Carbon particles, such as those created by combustion processes, are efficient adsorbers of many organic compounds and are able to carry toxic gasses such as sulfur dioxide into the lungs.

Presently there are no standards, indoor or outdoor, for respirable particulate concentrations (i.e., particles less than 3μm in diameter). The Environmental Protection Agency (EPA) does have an annual outdoor primary standard for total suspended particles (TSP) of 75 μg/m^3. However, since it is the fine particles that penetrate to the tracheobronchial and alveolar regions of the lung where adverse health effects are

most likely, the EPA is considering a new primary standard for inhalable particles (i.e., particles less than 10 μm in diameter) for outdoor air. It is not clear that such a standard would be appropriate for indoor exposures since, for example, the chemical and physical characteristics of indoor particles may be significantly different from those of outdoor particles.

Radon and Radon Progeny

Radon and its immediate decay products are ubiquitous contaminants of indoor air. Radon isotopes 222 and 220 (with half-lives of 3.8 days and 55 seconds, respectively) arise as part of the ^{238}U and ^{232}Th decay series, respectively, which are naturally occurring elements found in the earth's crust. In the United States at least, the dominant source of radon in homes is the underlying soil.

In this study we have employed ^{222}Rn and its decay products. Diffusion times from the soil limit the concentration of ^{220}Rn that can accumulate indoors in most situations; the average dose from ^{220}Rn progeny has been estimated to be about 25 percent of that from ^{222}Rn progeny (UNSCEAR, 1982).

Based on the limited data available, typical radon concentrations in U.S. housing range from 0.2 to 4 pCi/liter, averaged over a year (Nero 1983a). However, a number of houses in certain areas of the country have significantly higher radon concentrations, many in excess of 10 pCi/liter (Nero 1983b).

The most significant health risk associated with radon is the alpha decay of the two short-lived progeny, ^{218}Po and ^{214}Po. These elements, and the lead and bismuth isotopes shown in the ^{222}Rn decay chain in Figure 2, are chemically active and can attach to surfaces, such as airborne particles, walls, and lung tissue. A number of authors have modeled lung dosimetry due to radioactive decay of radon progeny (Harley and Pasternak, 1981; Jacobi and Eisfeld, 1980; James et al, 1981). While a detailed discussion of the models and results is beyond the scope of this paper, these models indicate that the alpha dose to the

lungs from progeny attached to aerosols is less than the dose from those progeny not attached to particles. The calculated dose due to unattached progeny for that area of the lung receiving the largest dose (basal cells in the bronchial tree) ranges from 9 to 35 times the calculated dose arising from attached progeny (James et al., 1981). Thus the fraction of unattached progeny is an important determinant in estimating the health effects associated with indoor radon concentrations.

II. WORKING PRINCIPLES OF PARTICULATE AIR CLEANERS

Particulate air cleaners can be separated according to their working principles into two different groups: mechanical filters and electrostatic filters. Mechanical filters remove particles from air as a result of mechanical forces imposed on the particle by the airstream and filter media. Electrostatic filters, on the other hand, rely primarily on electrostatic forces to remove particles from the air.

Mechanical Filtration

The removal of particles from air by mechanical filtration is generally accomplished by passing the air through a fibrous media. There are five basic mechanisms by which particles can be deposited on the fibers in a filter:

1. Inertial Impaction: The airstream being filtered makes an abrupt change in direction as it passes around each fiber in the filter. Particles of sufficient size collide with the fiber because of their inertia. This is the predominant means of collection for particles larger than 1.0 μm in diameter. Collection efficiency by inertial impaction increases with particle size and air flow velocity.

2. Interception: Interception occurs when a particle follows an air streamline that passes within one particle radius of the fiber. The particle makes contact with the fiber as it passes and is removed. Interception is the only collection mechanism that does not depend on air flow velocity and is an especially important removal mechanism for particles in the size range where minimum removal efficiency occurs. Collection by interception increases with increasing fiber density.

3. Diffusion: Brownian motion of small particles results from random collisions with surrounding gas molecules. This motion increases the probability of a particle hitting a fiber while traveling past it on a nonintercepting streamline. Diffusion is the only deposition mechanism that increases with decreasing particle size and is the predominant collection mechanism for particles smaller than 0.01

μm in diameter.

4. Electrostatic Attraction: As a charged particle passes close to an uncharged fiber it induces an equal and opposite charge on the surface of the fiber and the resulting electrostatic force attracts the particle toward the fiber. Similarly, when an uncharged particle approaches a charged fiber, the electrostatic image forces developed aid in the removal of the particle. The dielectric constant of the fiber material has an important effect on the development of image forces. Charged particles are also attracted to oppositely charged media by coulombic forces. These forces are much stronger than image forces and are the dominant collection force present in electrostatic filters.

5. Gravitational Settling: Gravitational settling of particles in fibrous filters is an insignificant removal mechanism for small particles (e.g., less than 1.0 μm in diameter).

The mechanisms of impaction, interception and diffusion predominate for different conditions of particle size and air velocity. The relationship between filter efficiency and particle size are shown in Figure 3 for a typical fibrous filter. For particles less than 0.01 μm in diameter, diffusion is the dominant removal mechanism while interception and inertial impaction dominate the removal of particles with diameters greater than 1.0 μm. The overall filter efficiency calculated from equations for diffusion and impaction reveals that there is a minimum efficiency at an intermediate particle size where the particle is too large for diffusion to be effective and too small for impaction or interception to be effective. Because these two mechanisms dominate in different size ranges, all filters have a particle size that gives a minimum efficiency. Depending on the fiber size, fiber density, and air flow rate the particle diameter at which the minimum efficiency occurs can range from 0.05 to 0.5 μm (see Figure 3).

Types of Mechanical Filters

Various types of mechanical filters are commercially available for use in unducted air cleaners. Three factors are important for characterizing the performance of these filters: the average fiber diameter, fiber packing density, and air flow rate. Increasing the fiber density increases filter efficiency at the expense of an increase in air flow resistance. The air flow in fibrous filters is generally laminar and thus air flow rate is directly proportional to the pressure drop across the filter.

Panel Filters: These filters have a low packing density of coarse glass fibers, animal hair, vegetable fibers, or synthetic fibers. The fibers in these filters are often coated with a viscous substance, such as oil, which acts as an adhesive for impinging particles. These filters are characterized by low pressure drop, low cost, and high efficiency for very large particles such as lint, but have a negligible efficiency for particles smaller than 10 µm in diameter. The common residential furnace filter is an example of this type filter.

Extended Surface Filters: Increased particle collection efficiency can be achieved by decreasing the fiber size and increasing the fiber packing density; however these measures also increase air flow resistance. By extending the surface area of the filter media, the air velocity through the media is reduced, which in turn reduces the pressure drop across the filter. One way of extending the media surface area is to deploy the media in a folded or pleated form. The larger ratio of medium surface area to face area in these filters allows use of denser and hence more efficient filter media while maintaining acceptable pressure drops. Extended surface filters also offer much higher dust holding capacities.

HEPA Filters: High Efficiency Particulate Air (HEPA) filters are special types of extended surface filters characterized by a very high efficiency in removing submicron particles. Initially developed for use in nuclear material processing plants to control concentrations of fine airborne radioactive particles, a HEPA filter is defined as a disposable

dry-type extended-surface filter having a minimum particle removal efficiency of no less than 99.97% for 0.3 µm diameter particles and a maximum pressure drop, when clean, of 1.0 inches of water (IWG) when operated at rated airflow capacity (Institute of Environmental Sciences, 1968). The filter core is generally constructed by pleating a continuous web of filter media over corrugated separators that add strength to the core and form air passages between the pleats. HEPA filter media are composed of very fine submicron glass fibers in a matrix of larger diameter (1-4 µm) fibers. A number of grades of high efficiency fibrous filters are commercially available with minimum efficiencies ranging from 95 percent for hospital grade to 99.99 percent for HEPA grade.

Electrostatic Filtration

Various electrostatic filtration processes have been developed for removing particles from air. While removal as a result of mechanical effects such as diffusion and inertial impaction still occurs to some degree, the major removal mechanism is electrostatic attraction. As a class these devices are characterized by a low pressure drop which is nearly independent of dust loading and by high efficiency for removing small particles. Three topics which are important for understanding the operation of electrostatic filters are air ionization, particle charging, and particle migration velocity.

Air Ionization: A convenient method of creating a large source of ions for particle charging in electrostatic filters is to produce a corona discharge by supplying a high voltage to a thin wire or a sharply pointed electrode. The high voltage creates an electric field that is sufficiently strong near the surface of the wire to ionize gas molecules. In this region, called the corona, free electrons are accelerated sufficiently to strip electrons from surrounding gas molecules creating positive gas ions and additional electrons. These additional electrons are, in turn, accelerated and cause further impact ionization. This chain-reaction process, called a corona discharge, produces large quantities of electrons and positive ions. If the electrode is positive, the electrons will move rapidly to the electrode and the positive ions will stream away from the wire. If the electrode is

negative, the positive ions will be attracted to the electrode and the electrons will be repelled. These free electrons then attach to electronegative gasses such as oxygen and water vapor thereby producing negative ions. Because of the high energies in the corona region, it is possible for some ozone, an air contaminant, to be produced from oxygen. Most electrostatic devices designed for cleaning indoor air use a positive corona since this polarity produces less ozone than a negative corona.

Particle Charging: Two mechanisms by which particles can acquire charge are diffusion charging and field charging. In diffusion charging, the particles pick up charges as a result of the random collisions between the ions and particles. Field charging results from collisions of particles with the rapidly moving ions in a strong electric field. The ions move along the electric field lines and strike particles which intersect those lines. The charge acquired is directly proportional to the particle diameter for diffusion charging and to the particle diameter squared for field charging. Field charging is usually the dominant charging mechanism for particles with diameters larger than 1.0 μm while diffusion charging usually dominates for particles smaller than 0.1 μm in diameter.

Particle Migration Velocity: The motion of a particle in an electric field is governed primarily by electrostatic and aerodynamic forces. The terminal velocity of a particle due to these forces is called the migration velocity and is analogous to the settling velocity of a particle falling in a gravitational field. Migration velocity is directly proportional to the charge on the particle and the strength of the electric field. Figure 4 shows a typical plot of theoretical migration velocity as a function of a particle diameter. As can be seen from this figure, there exists for a given charging condition a particle size which has a minimum migration velocity. The increase in migration velocity as particle diameter decreases below 0.1 μm is largely a result of the decreased aerodynamic drag force (i.e. slip) experienced by these particles. The particle collection in electrostatic filters is determined primarily by the particle migration velocity, collection surface

area, and air flow rate.

Types of Electrostatic Filters

There are three different types of electrostatic devices produced for removing airborne particles :

1. Ionizing flat-plate precipitators: This type of air cleaner is often referred to as an electrostatic precipitator. Most residential electrostatic precipitators are two stage precipitators, that is, they have a separate ionization stage preceding the precipitation stage (see Figure 5). Airborne particles are first charged by ions produced with an electric corona and then collected as they pass between a series of alternately charged and grounded collection plates. The collection efficiency of electrostatic precipitators can be increased by increasing the collector plate area, or decreasing the airstream flow rate. Similarly, increasing the particle migration velocity, by increasing the charge on the particle or the electric field strength, will increase collection efficiency. As seen in Figure 4, for a given charging condition there exists a particle size that results in a minimum migration velocity. Precipitators designed to capture this size particle with 100% efficiency will be 100% efficient for all particle sizes.

2. Charged-Media Filters: The charged-media air cleaner combines certain characteristics of both mechanical and electrostatic filters. These devices augment the normal mechanical removal mechanisms attributed to fibrous filters by charging the fibers. Airborne particles passing close to the charged fibers are polarized and drawn to the fibers by electrostatic forces. Charged-media filters which use a high voltage power supply normally use a filter medium constructed from a dielectric material such as glass or cellulose fibers. A gridwork of alternately grounded and charged members is in contact with the medium thus creating an intense and nonuniform electrostatic field.

A new filter medium that is gaining popularity among manufacturers of air cleaning equipment employs a special fibrous material which is embedded with permanent electrostatic charges called "electrets". Electret filter medium is manufactured by charging with a corona discharge the upper and lower surfaces of a thermoplastic film during the extrusion process. The electret film is then fibrillated, carded and needle punched into a finished nonwoven media. Similar to the externally charged media, electret media offer increased particulate removal efficiency as a result of the electrostatic forces imposed on the particles but requires no high voltage power supply. Tests performed with charged filter media have demonstrated high particulate removal efficiencies with relatively low pressure drops, however, there is some controversy regarding their performance after they have become loaded with particles.

Charged-media filter devices may also include an ionization stage where particles are first charged in a corona-discharge ionizer, then collected on a charged-media filter mat. This configuration provides higher efficiencies than would be possible if the charged media was used without a preceding ionization stage.

3. Ion Generators: While not a filter in the same sense as are other air cleaners, ionizers remove particles by charging them, after which they are attracted to surfaces at or near ground potential, such as walls, table tops, draperies, occupants, etc. In some cases, an oppositely charged collection surface is integrated as part of the device, which, in principle, reduces the problem of soiling of surfaces.

III.DESCRIPTION OF AIR CLEANERS TESTED

We evaluated eleven different devices. These included 4 panel-filter devices, 2 extended-surface filter units, 2 electrostatic precipitators, and 2 negative-ion generators. In addition we evaluated the effect of oscillating desk top fans on particle and radon progeny removal. Compiled in Table 2 are data summarizing our measurements of airflow rates and power consumption of the devices tested. Figure 6 is a photograph of nine of the eleven air cleaning devices tested (one of the negative ion-generators and the circulating fans we tested are not included in the photograph).

The four panel-filter devices we tested ranged in retail price (1983) from $30 for the Rush Hampton 7305 to $150 for the Neolife Consolaire. Each of these units has a small fan which draws or pushes air through a thin flat panel of filter media. The filtration media may be either uncharged or charged. Charged electret filter media is used in the Norelco, Pollenex, and Neolife devices while a relatively porous foam filter is used in the Rush Hampton unit. The Neolife Consolaire also incorporates a pair of negative ion-generators with electrode voltages of -3.4 kV just upstream of the filter medium. The maximum air flow rates in these devices were relatively small, ranging from 10 to 29 cfm.

The two extended surface filters we tested were the $295 Bionaire and the $395 Summit Hill Hepanaire. The Bionaire uses approximately 2.3 ft^2 of electret filter media folded into a 0.6 ft^2 face area (i.e. 3.8 ft^2 media/ft^2 face). The Summit Hill Hepanaire uses a glass fiber HEPA filter with a much larger surface area to face area ratio (i.e. 32 ft^2 media/ft^2 face). The Bionaire also has a negative ion-generator with an electrode voltage of -6.1 kV located just behind the airstream discharge grill. The air flow rates ranged from 29 to 66 cfm for the Bionaire, and from 102 to 202 cfm for the Hepanaire.

The two electrostatic precipitators we tested were the $370 Trion Console and the $395 Summit Hill Micronaire P-500. Both units are two stage flat-plate electrostatic precipitators and both use positive voltage for ionization. The collection stage of both units consists of alternately charged and grounded plates. A single high-voltage D.C. power supply is used to charge both the ionization electrodes and collection plates. The Trion device operates at 6.2 kV DC and has a total collector surface of 10.5 ft^2 compared with 6.5 kV DC and a 12.9 ft^2 collector surface for the Summit Hill unit. The air flow rates ranged from 146 to greater than 250 cfm for the Trion console and from 120 to 255 cfm for the Summit Hill Micronaire.

The two ion-generators we tested both generate negative ions. The ISI Orbit is a table top residential type ionizer which has an electrode voltage of -19 kV D.C. The Zestron Z-1500 is a ceiling-hung commercial-type ionizer which has an electrode voltage of -32 kV D.C. In addition, the ISI Orbit includes a 7.8 kV positively charged collection surface just beneath the ion-emitting electrode. According to the manufacturer this is designed to help collect the charged particles and thereby reduce soiling of indoor surfaces, since staining of indoor surfaces is one of the big complaints about ionizers.

The Dayton oscillating fan, model 4C507, we utilized is a typical multi-speed desk top circulating fan. The blade diameter is 12 inches and the air flow rate reported by the manufacturer ranges from 1325 to 1800 cfm.

IV. EXPERIMENTAL PROTOCOL

Air Cleaning Performance Parameters

Currently there are no standard methods for testing or rating portable air cleaners. The American Society of Heating, Refrigeration, and Air Conditioning Engineers (ASHRAE) have a standard testing procedure (ASHRAE, 1976) for evaluating ducted devices but in its present form it is not applicable to the evaluation of unducted devices. Furthermore the ASHRAE tests for arrestance and dust-spot efficiency do not give specific information regarding the efficiency of removing respirable-size particles. Several researchers have used in situ measurement techniques which are appropriate for evaluating the performance of portable air-cleaning devices (Offermann, et.al., 1983, Whitby, et.al., 1983). The test procedures normally involve filling a room-size chamber with a contaminant, mixing to obtain a uniform initial concentration, and measuring the contaminant decay rate with and without the air cleaner operating. The increase in the contaminant decay rate observed with the device operating can be used as a performance indicator for the device. If the flow rate of air through the device is known, an efficiency may be calculated.

The results of a chamber decay experiment can best be understood by reviewing the various contaminant source and removal terms involved. The contaminant decay rate in a chamber of volume V is described by the following differential equation;

$$\frac{dC_i}{dt} = \frac{S}{V} + \frac{PQ_I C_o}{V} - \frac{Q_I C_i}{V} - k\,C_i - \frac{nQ_D C_i}{V} \qquad (1)$$

where

C_i = the indoor concentration,

t = time,

S = indoor source term,

V = chamber volume,

P = penetration factor (dimensionless),

Q_I = infiltration or ventilation air flow rate,

C_o = the outdoor concentration,

k = contaminant reactivity,

η = device removal efficiency (dimensionless)
    ($\eta = 1 - C_{in} / C_{out}$), and

Q_D = device air flow rate.

This equation follows from the principles of conservation of mass and is based on the assumption of perfect mixing within the chamber; however, the assumption of perfect mixing is not necessary to calculate contaminant removal rates if measurements are made over a long enough period of time and if the air flow patterns are relatively constant. Figure 7 illustrates the various terms of Equation (1). The two sources of indoor contaminants considered in this model are S, an indoor source term, and $PQ_I C_o$, and outdoor source term which is the product of the infiltration air flow rate Q_I, the outdoor concentration C_o, and a penetration factor P. The three removal mechanisms considered are removal with the exfiltrating air, $Q_I C_i$, removal by all other natural reactive mechanisms (e.g. physical deposition, coagulation, chemical transformation), kC_i, and removal by the air cleaning device $\eta Q_D C_i$, which is the product of the device removal efficiency η, the device air flow rate Q_D, and the indoor concentration C_i.

For a chamber decay experiment where there is no internal source and where the outdoor aerosol source, $PQ_I C_o$, is negligible, the mass balance equation simplifies to;

$$\frac{dC_i}{dt} = -kC_i - \frac{\eta Q_D C_i}{V} - \frac{Q_I C_i}{V} \qquad (2)$$

If two tests are made, one with and one without the air cleaner operating, and if we assume that the exfiltration and reactive removal terms

are the same for both tests, then the difference between the observed decay rates represents the air cleaner removal term $\eta Q_D C_i / V$.

For processes such as particulate filtration where the removal efficiency, η, is normally considered to be independent of concentration, efficiency is calculated by multiplying the difference between the two measured decay rates by the chamber volume, V, and dividing by the device air flow rate, Q_D. If the chamber is perfectly mixed, and all source and removal terms remain constant for both measurements, then the calculated efficiency describes the actual device efficiency (i.e. one minus the ratio of outlet and inlet concentrations). If the chamber air is not perfectly mixed, then the decay rate measured at any one particular location reflects both the ventilation efficiency and contaminant removal efficiency, the sum of which can be called the "system efficiency" as opposed to the device efficiency. Sandberg (1981), Malstrom (1981), and others have shown that with imperfect mixing of indoor air and an initially uniform tracer or pollutant concentration, the decay rate initially varies from location to location but eventually attains the same value at all locations. The equilibrium decay rate then indicates the overall average contaminant removal rate. Thus in an imperfectly mixed system, the transient analysis described above results in the effective performance of the device which includes both device and ventilation efficiencies. Since the inlets and outlets of unducted devices are in such close proximity we have included the effects of imperfect mixing (i.e. short circuiting between inlet and outlet) in our performance measurements.

Two parameters we calculate from our measurements for each device are the effective cleaning rate (ECR), and the system efficiency. The ECR is the difference in the observed decay rates with and without the air cleaner operating multiplied by the chamber volume. This calculation gives an air flow rate that represents the effective amount of 100% particle free air produced by the air cleaner. The number is particularly useful when estimating the effects of the device in various size rooms. The system efficiency of an air cleaner is the ECR divided by the actual device airflow rate. This number is useful when comparing

the performance of different air cleaners or when evaluating the performance of a specific cleaner as a function of particle size.

Test Space Description

The experiments were carried out at the Indoor Air Quality Research House (IAQRH) located at the University of California, Richmond Field Station. The research house (see Figure 8) is a two-story, wood-frame structure containing a three-room test space that has been extensively weatherized to reduce the infiltration rate below 0.1 ach. Tests of the unducted control devices were performed in one room within this test space; a floor plan of this room is shown in Figure 9. The interior of the room, measuring 3.4 by 4.6 m by 2.3 m high, is constructed of plasterboard for three walls and the ceiling, and plywood sheathing for the fourth wall. All these interior surfaces are painted white. The floor is covered with sheet vinyl.

The approximate locations of sources, instrumentation, particle and radon sampling points, and the control device under test are indicated in Figure 9. A cigarette smoking machine (Arthur D. Little, Model ADL II Smoking System), modified to include an automatic extinguishing feature, was located at position 5. The duration of cigarette combustion was controlled by a timer that initiated the cigarette extinguishing sequence after a preset interval (usually six minutes). In-situ instruments for the measurement of particle-mass concentration and radon progeny concentrations were located on a table at position 2. Radon injection and sampling points for radon and particles were co-located at the center of the room, with the ends of the sampling lines positioned approximately 1.8 m above the floor. Indoor temperature and relative humidity probes were located near the center of the room.

The unducted control devices were either table-top models, which were placed on a small wooden table located at position 3, or larger, console-type devices (the size of a typical stereo speaker), which were usually placed directly on the floor at position 3. Some devices were also tested at an alternative location - position 4 - near the center of the room in order to minimize possible effects of nearby walls.

Tests were conducted using tobacco smoke as a source of combustion particles because 1) it is one of the most prevalent indoor particulate contaminants, 2) it is easily generated, and 3) it provides a polydisperse aerosol with a repeatable size distribution spanning the size range of respirable particles. Tobacco smoke is also an indoor contaminant for which most manufacturers of portable air cleaners have made performance claims. A scanning electron micrograph of cigarette smoke particles encapsulated and captured on a nuclear pore filter (Otto, 1983) is presented in Figure 10.

Instrumentation

The instrumentation employed in these tests comprises a highly automated data acquisition, monitoring, and control system installed at the IAQRH. It is designed to yield real-time data on particle, radon, and radon progeny concentrations, and environmental parameters and to provided programmable control over the operation of the experiment. Instrument control and data acquisition are done by two micro-computer systems. The first, referred to as the IAQ Research House Computer, is located in a room adjacent to the test space. A block diagram of this computer system is shown in Figure 11; its general operation is described elsewhere (Nazaroff, 1981). This computer performs both data retrieval and control functions. Data are stored by a cartridge magnetic tape recorder (Columbia Data Products tape deck Model DC300D) and are simultaneously printed by a terminal (Teletype, Model TTY 43). The operation of the various systems under computer control can be pre-programmed or directly executed during the course of the experiment. As indicated in Figure 11, the computer controls radon injection into the test space, particulate control-device operation, and operation of mechanical systems within the test space, which include ventilation and mixing fans and the furnace system (which was not used in the one-room experiments described here).

Radon and Radon Progeny Measurements

Three continuous radon monitors (CRM) were used to measure radon concentrations in the test space; for these tests all three CRM's sampled from the same location in the test space. A fourth CRM monitored radon concentrations in the instrumentation room. The CRM's, consisting of flow-through scintillation cells coupled to a 5-cm diameter photomultiplier tube, are operated continuously and the data logged on tape by the IAQRH computer every 30 minutes. More complete descriptions of the CRM, designed and fabricated at LBL, are given in elsewhere (Nazaroff et. al., 1981a; and Thomas, 1979). Radon progeny concentrations were also measured in real-time, using a Radon Daughter Carousel (RDC) designed and built at LBL (Nazaroff, 1983). This automated device collects airborne radon progeny on a filter during a preset sampling time (usually five min.), then places the filter beneath a surface-barrier detector, which separately counts the collected alpha radioactivity from ^{218}Po and ^{214}Po using spectroscopy. A radon progeny sample is collected every 30 min. during the experiment, with data recorded on magnetic tape via a link to the IAQRH computer. Filter grab samples were also collected periodically during the experiment and analyzed using alpha spectroscopy to supplement these RDC measurements.

Particle Measurements

Instrumentation for determining particle size and concentration is located on the second floor of the IAQ Research House and is connected to the test space via a 6 m long, 1 cm diameter copper sampling line. A schematic diagram of the particulate instrumentation and sampling manifold is shown in Figure 12. Air is drawn continuously from the test space, through the instrumentation manifold at ~5 l/min, and then exhausted back into the test space. Total aerosol concentration is measured with a condensation nucleus counter (CNC) (TSI, Model 3020). The CNC is also used to sample the output concentration of the electrostatic classifier (EC) (TSI, Model 3071); this procedure provides particle size and concentration data for particles with diameters between 0.01 and 0.3 microns. The optical particle counter (OPC) (PMS, Model LAS-X) has a dynamic range specially adapted to measure particle size

and concentration in the size range from 0.1 to 3 microns. A photograph of the particulate instrumentation and manifold sampling system is presented in Figure 13.

Control and data logging for particulate instrumentation is provided by the second micro-computer system -- the Particle Instrumentation Control System (PICS) computer shown schematically in Figure 14. This computer can control the sequencing of the sample line valves; however, since only one sampling line was used for these single room experiments, the position of the sample line valves remained fixed. The particle measurement sequence is begun by simultaneously initiating data acquisition by the OPC and positioning the three-way valve on the input to the CNC for sampling directly from the manifold. After a preset time to allow for flow stability, the computer reads the CNC output, records the total particle number concentration on tape, and repositions the three-way valve to sample the output aerosol from the EC. The computer controls the voltage applied to the central rod of the EC (which, for a given set of flow parameters, determines the particle size in the EC output) and the number of voltage steps in the EC measurement sequence. The CNC reading for each pre-programmed classifier voltage step is accumulated by the computer. At the end of the measurement sequence (the length of which is largely determined by the number of sequential EC voltage steps), the PICS computer records the accumulated CNC data on tape, then removes the data enable signal to the OPC. The OPC is essentially a stand-alone device with an internal buffer for data accumulation; at the end of the measurement sequence the accumulated data are written directly to the magnetic tape. Air flow through these instruments are monitored using several flowmeters whose analog signals are periodically recorded by the computer.

Aerosol mass concentration is monitored at fixed intervals by a Piezobalance (TSI, model 3500), located in the test space; the piezo-electric oscillations provided by the Piezobalance are read at the beginning and end of the preset mass measurement time by a frequency counter in the PICS. These two frequencies are stored on magnetic tape; the frequency shift during the measurement period is proportional to the

mass accumulated on the piezoelectric crystal. In order to prevent continuous accumulation of particles on the surface of the crystal, power for the corona discharge was gated off for pre-programmed intervals by the computer.

Airflow Rate and Power Consumption Measurements

Airflow rate and power consumption measurements were made at each speed setting of each particle control device. The airflow rate measurements were made using an orifice plate flowmeter constructed in accordance with American Society of Mechanical Engineers specifications and installed in a 6-m length of 10-cm-diameter PVC pipe. A blower was installed on one end of this pipe to move air through the pipe and orifice plate. The intake of the air-cleaning device was connected to the other end of the pipe with a 1 m long lightweight polyethylene bag. Measurements were made by turning the device and blower on and adjusting a valve in the pipe so that the static pressure in the polyethylene bag was zero. Thus the airflow rate through the device was not affected by the attachment of the orifice plate system. Fan power consumption was measured using an AC wattmeter (Weston Instruments).

Test Procedure

Testing of each unducted device typically followed a 24-hour time sequence, which is summarized in Table 3. The instrumentation and data logging remained in operation throughout the 24-hour period. The cigarette smoking machine and extinguisher were on a timer; thus after manual ignition of the cigarette, the test space was not entered again during the test sequence. A smoking rate of two 35 ml puffs per minute was used and both main-stream and side-stream smoke from the cigarette smoking machine were emitted into the test space. A typical six-minute cigarette burn consumed ~600 mg of tobacco and produced a peak concentration of ~1 to 2 x 10^5 particles/cm^3, corresponding to a peak mass concentration of ~ 400 µg/m^3.

After cigarette ignition, radon was injected into the test space by passing air through a volume containing 115 microcuries of emanating ^{226}Ra precipitated as a solid stearate and captured between two filters. The radon is typically allowed to accumulate in the source for 24 hours and is then injected into the 36 m^3 test space, resulting in an initial radon concentration of ~500 pCi/l. The air in the room was allowed to mix naturally and the particle and radon concentrations allowed to decay for a four-hour period, which allowed an equilibrium particle decay rate to be established, and is also sufficient time to achieve radioactive equilibrium of the radon decay products.

Following the decay and mixing period, the control device was turned on, usually for three to five hours depending upon the effectiveness of the device. After control device operation, a six to eight hour period of natural decay ensued, which provided another measurement of the natural decay rate for particles. The test space was then ventilated for a three to four hour period using the range hood. While no direct control of relative humidity (RH) was possible during the test without interfering with the particulate removal processes, a portable dehumidifier was operated for a four to five hour period preceding the test to produce an initial RH of 35 to 50 percent. The humidity then slowly increased by 10 to 15 percentage points during the 24-hour test sequence.

V. RESULTS AND DISCUSSION

In this section, we present the results of the particle and radon progeny measurements in separate subsections. Within each subsection, the necessary mathematical developments are shown as a component of the data analysis procedure, followed by results and discussion.

A. Particles

Data Analysis Procedures

To calculate the effective cleaning rates and system efficiencies for each air cleaner the data were first organized as semi-logarithmic plots of particle concentration as a function of time, where the slopes of the lines then represent the decay constants. Figures 15 and 16 present data for two of the eleven devices we tested; Figure 15 shows results from a test of a HEPA-type air cleaner, while Figure 16 depicts a test of a small panel-filter air cleaner. As we shall explain below, this latter figure is also representative of data obtained for each of the panel-filter devices we tested as well as one of the negative ion generators. We also performed a 'no device' experiment, and data obtained from that test is also similar to that shown in Figure 16. The top line in each of these figures is the total particulate concentration as determined by the CNC, and the lower four curves are particle concentrations in size ranges measured selected by the optical particle counter.

Since the calculations of effective cleaning rates require measurement of the steady state-decay rates with and without the device operating, it is necessary first to determine when the natural decay rates have reached steady state. Following injection and the initial rapid decay period (especially apparent for particles smaller than 0.3 μm diameter), a steady decay rate soon develops, as can be seen in Figures 15 and 16. Similarly there exists a short transition period following activation of the air cleaner before the decay rate becomes constant. We use the linear portion of the (semi-logarithmic) decay curves as the basis for our removal rate calculations. With air cleaners having high

particle removal rates, the observed particle concentrations decay very rapidly to values two to three orders of magnitude lower than the initial concentration. The particle concentration eventually equilibrates when the removal rate balances the production rate, which is roughly that expected from the 0.05 hr^{-1} infiltration rate for outside air.

The decay constants for the natural and control periods of each experiment were calculated by fitting the experimental data to an exponential curve using a precision-weighted least squares regression (Picot, 1980). The quality of the fit was then checked by calculating the 90% confidence limits of the decay constants (Bowker and Lieberman, 1972).

Uncertainties in the ECR arise from several sources. Uncertainties due to measurement of particle concentration do not affect the ECR, if we assume that the measurement accuracy of the instruments are independent of time (i.e. no drift) and concentration change (i.e. negligible changes in counting efficiency). This also assumes that any remaining systematic errors in the measurement of particle concentrations are percentage errors, and thus cancel when the decay rates are computed. With these assumptions, the major source of uncertainty in our decay rate calculations arises from the number of data points and the degree of fit of the decay curves to the data points. The uncertainty in the volume measurement was estimated to be ±4%. For calculating system efficiencies, we estimated the uncertainty in our flow rate measurements to be ±10%. The uncertainties associated with each measurement were assumed to be independent of one another and were added together in quadrature to obtain the uncertainties for the various performance parameters.

Results of Particulate Measurements

Particulate measurements were made for twenty two different size ranges, however, only eleven of these size ranges contained data of sufficient precision to be useful in calculating decay rates. Data from the six channels of the electrostatic classifier (i.e. 0.005 to 0.20 μm diameter) were inconsistent over time during a number of the experiments. In addition, data from the five largest channels of the optical

particle counter are not included in our analyses because of the poor counting statistics associated with the relatively low concentrations of particles above 1.25 μm diameter. Thus, our measurements of effective cleaning rates and system efficiencies as a function of particle size are based on eleven channels of the optical particle counter which span the particle size range of 0.09 to 1.25 μm diameter.

Typical aerosol number size distributions for tobacco smoke are presented in Figure 17 for five measurement times during a natural decay experiment conducted without an air cleaner operating. The figure also shows the data from one of these measurements converted to a mass size distribution assuming spherical particles with a density of 1 gm/cm^3. Concentrations in particles/cc are normalized by the logarithm of the width of the particle size bin. The data obtained with the electrostatic classifier (i.e. less than 0.09 μm diameter) have been normalized to the OPC data at a particle diameter of 0.20 μm, where data from the two instruments overlap. Typically, the tobacco smoke aerosol had a near log-normal size distribution with a geometric count median diameter of 0.15 μm and a geometric standard deviation of 2.0. Other researchers have reported log-normal distributions for tobacco smoke, with geometric count median diameters ranging from 0.1 to 0.5 μm (Hinds, 1978).

The size distribution measured at 10:01 represents the background aerosol normally present in the test room. The four sharply peaked distributions represent successive measurements following the smoking of a cigarette at 10:25. The effects of decay rate on the aerosol size distribution can be seen by comparing the four different curves. A significant decay in number concentrations of particles less than 0.1 μm diameter can be observed, while for particles with diameters greater than 0.2 μm there appears to be much slower decay in concentration.

Figure 18 is a plot of the natural particle deposition rate as a function of size during this same experiment. Deposition rates were calculated as the observed particle decay rate less the decay rate associated with air exchange. The air-exchange rate, determined from the radon concentration decay rate (corrected for radioactive decay), was approximately 0.05 hr^{-1}. Since the indoor particle concentration was

much higher than the outdoor concentration the infiltration of outdoor air as a source of particles was not considered. For particles with diameters between 0.2 and 0.4 μm the natural particle decay rates are a minimum, 0.05 hr^{-1}. For particles with diameters less than 0.10 μm, diffusion is the dominant particle removal mechanism while gravitational settling is the most important removal mechanism for particles greater than 1.0 μm in diameter. Because these two mechanisms dominate in different size ranges, a minimum particle deposition rate occurs for particles with diameters between 0.1 and 0.5 μ diameters. The change in the size distribution noted in Figure 17 is partially the result of this dependence of deposition rates on particle size.

For comparative purposes, our effective cleaning rates are base on decay rates observed for 0.45 μm size particles. This size is close to the mass median diameter for cigarette smoke, and thus the corresponding decay rate is a reasonable index for the total mass decay rate of the aerosol.

Table 4 summarizes the test results and purchase and operational costs of the eleven air cleaning devices tested. Effective cleaning rates ranged from 0 cfm for the Rush Hampton panel filter device to 180 cfm for the Summit Hill HEPA-type filter unit. The least effective devices tested were the four small panel filters and the one residential negative ion generator, which had effective cleaning rates ranging from 0 to 7 cfm. The two circulating fans, which circulated 3600 cfm or 174 room volumes/hour, had virtually no effect on the removal of cigarette smoke. The two electrostatic precipitators tested had effective cleaning rates of 122 and 116 cfm. These effective cleaning rates are shown as the unshaded bars in Figure 19.

We should note that following all of our tests, even those where essentially all particulate matter was removed, there remained a strong odor of tobacco smoke. This odor results from gas phase contaminants produced by tobacco combustion and requires separate control measures (e.g. ventilation) for removal.

Discussion

One approach to putting our results into perspective is to consider the time it takes the air cleaner to remove 98% of the smoke from a room. The removal time is indicated on the right hand axis of Figure 19 for the 1241 ft^3 test space (e.g. 12x13x8 ft). The time periods range from 1/2 hour for the Summit Hill HEPA filter to more than 16 hours for any of the panel filters or the ISI Orbit negative ion-generator.

The measured air flow rates of each air cleaner are depicted in Figure 19 as shaded bars. The system efficiency for each air cleaner can be seen by comparing the unshaded and shaded bar for each device. As a class the most efficient devices tested were the two extended surface filter units. The efficiency of the Summit Hill Hepanaire was 115 ± 13% while the Bionaire 1000 had an efficiency of 86 ± 9%. The efficiencies of the two electrostatic precipitators were 57 ± 11% for the Trion Console and 58 ± 6% for the Summit Hill Micronaire.

Panel Filters: The low effective cleaning rates of the four panel filter devices can be attributed to a combination of low air flow rates and low particulate removal efficiencies. The airflow rates of these devices ranged from 10 to 29 cfm. If the filters in these devices were 100% efficient the effective cleaning rates would also range from 10 to 29 cfm, which means they would still require between 3 and 8 hours to remove 98% of the smoke in a 1241 ft^3 room. This is approximately the same rate at which tobacco smoke would naturally dissipate in a room with a ventilation rate of one air change per hour.

The Norelco, Pollenex, and Neolife panel filter units all use an electret filter media. While this type media is recognized to have moderate to high particulate collection efficiency depending on the thickness and fiber density, one reason it does not perform well in these devices is that a large percentage of the air entering the device bypasses the filter, due to a poor fit between the filter cassette and the device housing (see Figure 20). The higher efficiency of the Neolife panel filter unit, 39%, may be due in part to the addition of the negative ion generators just upstream of the media, however, because of

the very small flow rate of air through this air cleaner, about 17 cfm at medium fan speed, the effective cleaning rate is only 7 cfm.

Extended surface filters: The most efficient devices tested were the two extended surface filters. The high efficiencies of these devices results from minimal air by-pass and from use of a high efficiency filter medium. As can be seen from Table 2, the two high efficiency extended filters tested had relatively high air flow rates per watt of power consumed; 2.6 cfm/watt for the Bionaire and 2.3 cfm/watt for the Summit Hill Hepanaire.

The Summit Hill Hepanaire had a measured system efficiency of 115 ±13%. This air cleaner uses a high efficiency filter constructed from a high density of fine glass fibers, and is specified by the manufacturer as having a 95% efficiency for 0.3 μm diameter particles at the operating flow rates. The system efficiency of the Bionaire 1000 was 86 ± 9%. This air cleaner uses electret filter media in a three-fold convoluted format. In addition the Bionaire has a negative ion-generator. We did not separately evaluate the effect of this ionizer on particle removal.

Electrostatic Precipitators: The efficiencies of the two electrostatic precipitators we tested were less than those observed for the extended surface filters but still relatively high. The efficiency of the Trion Console air cleaner was 57 ±11% while the efficiency of the Summit Hill Micronaire was 56 ±6%. The effective cleaning rates were 122 ±19 and 116 ±5 cfm, respectively. The efficiency of moving the air through the electrostatic precipitator devices were similar to those found for the extended surface filters, 2.0 to 2.6 cfm per watt of power consumed.

While the performance of these two electrostatic precipitators for the removal of cigarette smoke is similar, we observed a sharp increase in total particle number concentration during operation of the Trion device that was not seen during tests with the Summit Hill unit. We noted this phenomenon in repeated tests with the Trion precipitator, but saw it only in the CNC output and in the small particle size channels of the electrostatic classifier; we saw no indication of an increase in

particle concentration in the OPC data. This increase in the concentration of very fine particles did not appear to affect the radon progeny concentrations, although based on the particle concentrations measured by the CNC some increase in radon progeny concentration would have been expected. We have no immediate explanation for these observations, although sparking in the electrostatic precipitator between the corona wire and the plate at ground potential could be a source of ultrafine particles, as could gas-phase reactions with ozone produced in the corona discharge.

Ionizers: We tested two ionizers. One was for residential applications, the Orbit model, manufactured by ISI Inc., and the other was designed primarily for commercial use, the Zestron Z-1500, manufactured by Zestron Inc. The Orbit is a negative corona ionizer with a positively-charged collection surface below the emitting electrode. One test of this device was performed with the ionizer located on a wooden-topped metal stool in the corner of the test space, at location 3 in Figure 9. The ECR for these conditions was 6 ±1 cfm. Moving the device to an all-wood table in the center of the room (position 4 in Figure 9) produced an ECR of 1 ±1 cfm, which we report in Table 4. It is possible that for the test with the device in the corner of the room, additional air cleaning resulted from deposition of some of the particles on the nearby walls and/or was due to the additional convective air flow along the wall surfaces that may have helped to circulate particles near the ionizer.

The effective cleaning rate for the Zestron Z-1500 ionizer, 30 ±1 cfm, was measured with the device suspended about 30 cm from the center of the ceiling (position 4 in Figure 9) and with the ionizer needles pointed toward the floor. The room air circulation conditions were similar for both the ISI Orbit and the Zestron Z-1500 tests. One possible reason for the difference in performance between the two ionizers may be related to the positively charged collection surface used with the Orbit. While we did not measure the ion flux lines coming from the Orbit it seems plausible that the field lines would be confined to a relatively small volume surrounding the corona discharge electrode and

the collector. This configuration while reducing the plate out of particles onto indoor surfaces also reduces the ion concentration produced in the remainder of the room.

Another factor which deserves consideration is the effect of particle charging on deposition in the human respiratory system. In experiments conducted by Melandri et. al. (1983) total respiratory deposition has been observed to increase linearly with an increase in the number of charges per particle. Further studies are needed to determine whether ionizers on balance reduce the dose to humans from inhaling particles.

Air Circulation: Two table top oscillating fans manufactured by Dayton were used to examine the effects of increased air circulation on particle deposition rates. The fans, operated at high fan speed, were positioned about 60 cm from the wall, and directed to blow air on the wall surface. The combined air flow rate was 3600 cfm or 174 room volumes per hour. There was no observable increase in the particle removal rate when the fans were operated.

Comparison with Results Reported by Others

Table 5 is a comparison of our measured Effective Cleaning Rates with data reported by two other laboratories. These data cover 28 different models of portable air cleaners, some of which were not evaluated directly by us, but are included to provide additional data on types of air cleaners. The data presented for Lab A are based on tests of twenty devices in a 1200 ft^3 chamber using tobacco smoke; these tests were performed by the staff at New Shelter Magazine (1982). Particle concentrations were measured using a photometer (GCA RAM-I Aerosol Monitor) during four-hour test periods with and without an air cleaner operating. Data presented for Lab B are from tests by Whitby, et. al, (1983) that were conducted in a 46 ft^3 glove box using a photometer to measure particle concentrations. Punk smoke was used as a source of test aerosol. Results from both labs are shown in terms of effective cleaning rate in Table 5.

Four models of air cleaners were tested by both LBL and Lab A; LBL and Lab B did not test identical air cleaner models (nor is there any overlap between models tested by Labs A and B). As can be seen from the data in Table 5, the results for identical models of air cleaners agree well except for the Orbit ionizer. Their result, 17 cfm, compared with our value of 1 ±1 cfm appears to be due to the continuous use of mixing fans within the test chamber during the Lab A tests. As we noted earlier, ion generators such as the Orbit rely on air circulation (either natural or externally-generated) to help transport charged particles to indoor surfaces. To test this hypothesis, we repeated our test of the Orbit using four-inch diameter wall-mounted mixing fans (with the fan axis parallel to the wall surface) which were operated continuously during the test period. Two different tests conditions were used, one with four fans operating (one fan per wall) and one using two fans (opposite walls). An effective cleaning rate of 10 ± 1 cfm was observed for both tests, which is higher than when no mixing fans were operated, but still lower than reported by Lab A. We note, however, that the mixing fans used for their tests were larger than our 4 inch fans, and had metal fan blades.

Since our test protocol was designed to test devices in a uniform manner, but under reasonably realistic conditions, we chose not to use mixing fans. Arguably, in a typical residence there are external air flows resulting from human activity, as doors are opened, etc. However, there are situations (or perhaps more accurately, times of the day) when such activity is minimal, but air cleaning may be desirable. Thus we have adopted a test procedure that does not rely on additional air movement. In this regard, the effective cleaning rates shown in Table 5 for the ion generators tested by Lab A may be substantially higher than are likely to occur in residences.

B. Radon and Radon Progeny

Before discussing the effects of particulate control devices on radon progeny concentrations, we first review the basic definitions and equations used in characterizing radon decay product concentrations and their attendant health risks. This is followed by a more detailed

development of the physical concepts and mathematical equations used to describe our results.

A commonly-used method of parameterizing the concentration of radon daughters in terms of the health risks due to their alpha decays is the Potential Alpha Energy Concentration (PAEC),

$$PAEC = \sum_{i=1}^{i=4} N_i \, E_i \qquad (3)$$

where N_i is the number concentration and E_i the potential alpha decay energy (in MeV) to ^{210}Pb, which, due to its 19.4 yr half-life, effectively terminates the radon decay chain for concern about lung cancer. The subscript i=1 to 4 refers to ^{218}Po, ^{214}Pb, ^{214}B; and ^{214}Po, respectively. The potential alpha energy for ^{218}Po is the sum of the alpha decay energy of ^{218}Po itself (E = 6.0 MeV) plus the alpha decay energy of its eventual ^{214}Po decay product (E = 7.7 MeV). The potential alpha energy is 7.7 MeV for each of the successive progeny ^{214}Pb, ^{214}Bi, and ^{214}Po.

Since one typically measures concentrations of radioactive species in terms of their radioactivity, substituting

$$A_i = N_i \, \lambda_i \qquad (4)$$

in Equation (3), where A_i is the activity concentration and λ_i the radioactive decay constant for the ith isotope, yields

$$PAEC = \sum_{i=1}^{i=4} \frac{A_i \, E_i}{\lambda_i} \qquad (5)$$

This quantity is given the units of "working level" (WL), and the measurement is often termed a working level measurement. For radon progeny in equilibrium with approximately 100 pCi/liter of radon, PAEC is 1.3 x 10^5 MeV/liter, which is defined as 1 WL. Another useful term is the Working Level Ratio (WLR), which is given by

$$WLR = 100 \frac{PAEC}{A_0}$$

<div align="right">(6)</div>

where A_0 is the corresponding (activity) concentration of radon (WLR is also referred to by some authors as the equilibrium factor). In the example just referred to, the WLR is 1 for the case of radioactive equilibrium among radon and its progeny. It turns out that this is rarely, if ever, achieved in a typical indoor situation, since (as we discuss at length in presenting our results) a number of factors tend to reduce the daughter concentrations, yielding working level ratios of less than 1.

Mathematical Background

Unlike removal of airborne particles, where ventilation, particle deposition and/or electromechanical filtration are the dominant removal processes for particle concentrations of less than 100,000 particles/cm^3, radon progeny have several additional removal modes. These are illustrated in Figure 21 with the rate for each process shown in parenthesis; Radon has two decay or removal mechanisms; radioactive decay to ^{218}Po, (λ_0), and removal by ventilation, (λ_V). There are five possible removal pathways for unattached (i.e., free) radon progeny: 1) ventilation, 2) removal by a control device,(λ_F^f), 3) plate-out on a macro surface, such as a wall, (λ_{po}^f), 4) attachment to an airborne particle, (commonly signified by X), or 5) radioactive decay to ^{214}Pb (not explicitly noted in Figure 21). The superscripts f and a refer to free and attached progeny, respectively. With the exception of radioactive decay, all removal processes are assumed to be independent of chemical species.

For progeny attached to aerosols, there is a similar set of removal possibilities: ventilation, removal by a control device, (λ_F^a), and deposition on a surface of the particle bearing the radionuclide, (λ_d^a). In the case of radioactive decay of ^{218}Po, which alpha decays to ^{214}Pb, the recoil momentum is sometimes sufficient to detach the decay product from the particle, with a detachment probability denoted as r. Analogously, one might expect a similar detachment process for ^{218}Po deposited on macro surfaces. However, the recoil range for ^{214}Pb is 0.15 mm

in air, which is within the boundary layer where diffusion-driven transport to the surface will result in a high probability of reattachment (Bruno, 1983). Hence we have assumed that recoil from these surfaces is negligible. No recoil detachment of ^{214}Pb or ^{214}Bi is expected since these nuclide are β-emitters.

We can now write down steady-state equations that describe these various decay modes, following the derivations of Jacobi (Jacobi, 1972) and Porstendoerfer (Porstendoerfer et. al., 1978a). There are two equations that describe the activity for each nuclide, one for the unattached species and one for the attached. The source terms are shown on the left, and the sink or removal terms on the right.

$$\lambda_1 A_0 = (\lambda_1 + \lambda_V + \lambda_F^f + \lambda_{po}^f + X) A_1^f \tag{7}$$

$$X A_1^f = (\lambda_1 + \lambda_V + \lambda_F^a + \lambda_d^a) A_1^a \tag{8}$$

$$\lambda_2 A_1^f + \lambda_2 r A_1^a = (\lambda_2 + \lambda_V + \lambda_F^f + \lambda_{po}^f + X) A_2^f \tag{9}$$

$$X A_2^f + \lambda_2 (1-r) A_1^a = (\lambda_2 + \lambda_V + \lambda_F^a + \lambda_d^a) A_2^a \tag{10}$$

$$\lambda_3 A_2^f = (\lambda_3 + \lambda_V + \lambda_F^f + \lambda_{po}^f + X) A_3^f \tag{11}$$

$$X A_3^f + \lambda_3 A_2^a = (\lambda_3 + \lambda_V + \lambda_F^a + \lambda_d^a) A_3^a \tag{12}$$

Since our measurements of progeny concentrations depend upon collection using filter samplers, they do not distinguish between attached and unattached decay products. The total activity, A_i, is given by,

$$A_i = A_i^a + A_i^f \tag{13}$$

and the unattached and attached fractions are,

$$f_i = \frac{A_i^f}{A_i} \qquad (14)$$

$$1-f_i = \frac{A_i^a}{A_i} \qquad (15)$$

Combining the pairs of Equations (7) and (8), (9) and (10), and (11) and (12), along with these definitions of unattached fraction, we can derive equations for the total airborne progeny activity for each species,

$$\lambda_i A_{i-1} = [\lambda_i + \lambda_V + f_i(\lambda_F^f + \lambda_{po}^f) + (1-f_i)(\lambda_F^a + \lambda_d^a)]A_i \qquad (16)$$

Substituting Λ_i for the sum of all the removal terms in Equation (16) except radioactive decay, we have

$$\lambda_i A_{i-1} = (\lambda_i + \Lambda_i) A_i \qquad (17)$$

which, when rearranged, gives us the total progeny removal rate for each isotope as a function of the measured activities,

$$\Lambda_i = \lambda_i [\frac{A_{i-1}}{A_i} - 1] \quad \text{where } i = 1,2,3 \qquad (18)$$

The subscripts 0, 1, 2, 3 refer respectively to ^{222}Rn and its progeny ^{218}Po, ^{214}Pb, and ^{214}Bi.

As can be seen from these equations, the combined removal rate, Λ_i, depends upon a number of variables. Some of these are measured directly in the experiments, as we note in greater detail below. It would be useful to have an expression for the unattached fraction, f_i, in terms of other variables that can be measured or estimated (in lieu of direct measurement of the unattached progeny concentration). Using Equations (14) and (15) above, we can divide both sides of Equation (8) by A_1, then rearranging the terms, we get

$$f_1 = \frac{L_1^a}{L_1^a + X} \tag{19}$$

where the variable L_i^a is given by

$$L_i^a = \lambda_i + \lambda_V + \lambda_F^a + \lambda_d^a \tag{20}$$

Similarly, dividing both sides of Equation (10) by A_2 and rearranging gives

$$f_2 = \frac{L_2^a - \lambda_2 (1-r)(1-f_1)(\frac{A_1}{A_2})}{L_2^a + X} \tag{21}$$

Dividing both sides of Equation (12) by A_3 and rearranging yields

$$f_3 = \frac{L_3^a - \lambda_3 (1-f_2)(\frac{A_2}{A_3})}{L_3^a + X} \tag{22}$$

Finally, to complete our discussion of the mathematical approach used in analysis of the radon and radon progeny data, we rewrite our previous definition of radon progeny concentration and working level ratio (WLR) given in Equations (5) and (6) in terms of the progeny activities,

$$WLR = \frac{k_1 A_1 + k_2 A_2 + k_3 A_3}{A_0} \tag{23}$$

where

$$k_i = 2.85 \times 10^{-5} \frac{E_i}{\lambda_{i,}} \tag{24}$$

for E_i in MeV/atom and λ_i in sec^{-1}. From Equation (18)

$$A_i = \frac{\lambda_i A_{i-1}}{\lambda_i + \Lambda_i} \tag{25}$$

-37-

which gives

$$WLR = \frac{\lambda_1}{\lambda_1 + \Lambda_1} [k_1 + \frac{\lambda_2}{\lambda_2 + \Lambda_2} (k_2 + k_3 \frac{\lambda_3}{\lambda_3 + \Lambda_3})]] \qquad (26)$$

Data Analysis Procedures

Radon and radon progeny data were accumulated every 30 minutes during the experiments. Typical activity concentrations for radon and radon progeny are shown as a function of time in Figures 22 and 23. Data obtained from the test of the HEPA-type filter are shown in Figure 22, while Figure 23 contains data from the test of a panel filter. Analysis of radon progeny behavior was based on progeny concentration measurements at two time periods. The first of these measurement periods was just before air cleaner operation. The second period was during operation of the air cleaning device, usually three hours after the device was turned on. For each of these time periods data from three sequential measurements were combined to determine the progeny concentrations after radioactive equilibrium had been established.

In analyzing the data, it became apparent that at low particle concentrations (resulting in very low working level ratios, as we discuss below), data from the radon daughter carousel (RDC), located in the test space, did not agree with data obtained from grab sample measurements. It appears that the problem arises because the sampled daughter activities are so low compared with the radon-related background. In the counting position in the RDC, there is an air gap between the filter and the surface barrier detector. Radon within this gap decays, contributing to the background in the alpha decay spectrum, and depositing additional radon progeny either on the filter or detector surface. In those cases in which the particulate concentrations were less than a few hundred particles/cm^3, we have relied on data taken with a filter grab sampler to yield radon progeny concentrations. The filters were analyzed using a two-count period, alpha-spectroscopic method essentially the same as employed in the RDC (Nazaroff, 1983a).

Results of Radon and Radon Progeny Measurements

For each set of radon and radon progeny measurements made either before or at the end of the device operation we have tabulated in Table 6 the particulate concentration, the total progeny removal rate, Λ_i, based on Equation 18 above, and the corresponding working level ratio. These experimentally-determined working level ratios are also shown in Figure 24 as a function of particle concentration. The representative uncertainties indicated in Figure 24 are based on uncertainties due to counting statistics.

As can be seen from Equations (16) and (17), the total removal rate Λ_i includes removal by ventilation, unattached progeny plateout, deposition of attached progeny, and, for data taken during device operation, removal of attached and unattached progeny by the control device. Several of these quantities are either measured directly, or inferred from our data; these parameters are summarized in Table 7. The ventilation rate for the test space can be obtained directly from the radon concentration data measured during the course of the experiments. For most of the single room tests described here, the average rate of change in radon concentration (corrected for radioactive decay) is 0.05 hr^{-1}. The particle deposition rates are based upon the particulate mass balance shown in Equation (1), where the term kC_i represents particle removal by natural mechanisms, such as deposition, coagulation and chemical transformation. Under the conditions used for these experiments, the latter two removal mechanisms are negligible. Figure 18 above shows the particle decay rate, which we attribute to surface deposition, as a function of particle size. Based on measurements of total particulate (number) concentrations with the CNC, the average value of k, which we equate with λ_d^a, is 0.16 hr^{-1}. This result, obtained under conditions of minimum air circulation, is consistent with reported values of 0.1 hr^{-1} and 0.2 hr^{-1} (Porstendoerfer et. al., 1978a) and (Wicke and Porstendoerfer, 1982), respectively. It is somewhat smaller than 0.34 hr^{-1} used by Scott (Scott, 1983) and slightly larger than the value of 0.05 hr^{-1} used by Knutsen (Knutsen et. al., 1983).

In our equations for Λ_i and f_i, we have included separate terms for the attached and unattached progeny removal rates for the control devices. For the attached progeny removal rate, $\lambda_F{}^a$, we have used our measured values for the particulate removal rates for each device. For the unattached progeny the airborne species are expected to be small molecules, such as metal oxides, with molecular sizes on the order of 5 nm (see, for example, Busigin, 1981; Knutsen, 1983). Since these sizes are below the measurement capabilities of the present experiments, we assume that the removal rate for unattached progeny is the same as for attached progeny. Since the HEPA filter has a <u>minimum</u> device efficiency of nearly 100 percent, removal rates for unattached and attached progeny must be almost identical. For the electrostatic devices our assumption of equal removal rates for attached and unattached progeny is less certain.

We now turn our attention to the calculation of the fraction of radon progeny that are unattached (the "free fraction"). In addition to the quantities we have measured directly or estimated from our results, f_i depends upon two other parameters: the rate of attachment X, of the unattached progeny atom or molecule to the ambient aerosol, and for the case of ^{218}Po alpha decay to ^{214}Pb, the recoil detachment probability r. Porstendoerfer and Mercer(1978b) have measured attachment rates for ^{220}Rn (thoron) progeny to indoor and outdoor aerosols, and found a linear relationship between attachment rate, X, and particle concentration for concentrations between 0.6 and 7 x 10^4 particles/cm^3 . Although the attachment rate depends upon particle size, based on their measurements they arrive at a mean attachment rate coefficient of 4.3 x 10^{-3} hr^{-1} x (particles/cm^3)$^{-1}$. We use their formulation for X as a function of particle concentration, recognizing that there are uncertainties due to our extrapolation to lower particle concentrations and due to possible differences in the physical and chemical characteristics in the aerosols used in the respective experiments. For the recoil probability, r, we have adopted the estimate of 0.83 made by Mercer (Mercer, 1976).

Our estimates for the unattached fraction for each radon decay product are shown in Table 8 based on the results of each control device test. We have also tabulated the particle concentrations measured before and at the end of the period of control device operation, the calculated value for the attachment rate, X, and our measured particle removal rate due to operation of the control device. The unattached fractions are plotted as a function of particle concentration in Figure 25. The lines drawn through the data points serve as guides to the eye. We have also indicated in Figure 25 the range in the uncertainty in our estimates for f_i based upon assumed uncertainties in the attachment rate, X. For particle concentrations above 5000/cm^3, we show the effects of a 20 percent uncertainty in X as error bars on the unattached fractions at 35000 particles/cm^3. A twenty percent uncertainty in X at low particle concentrations would yield uncertainties in f_i the size of our data points. The error bars shown at 45 particles/cm^3 are based on an assumption of an order of magnitude uncertainty in X for these low particle concentrations.

We can now estimate the plateout rate for free radon progeny based upon our measurements and the estimates of the free fractions we have just made. From Equation (18) and our definition of Λ, λ_{po}^f can be derived in a straightforward manner. One can also see from Equations (21) and (22) that f_2 and f_3 depend not only upon our assumptions about X, but also depend upon the free fraction for the parent nuclide, and the measured ratio of parent and decay product activities. For some particle concentrations, the numerator in these equations then becomes the difference between two nearly equal numbers, and the uncertainty in f_2 and f_3 increases correspondingly. As a consequence, we have used the data and equations for ^{218}Po only in our estimates for the free plateout rate. We then assume for subsequent calculations that λ_{po}^f is independent of progeny species. Based on these estimates, we derive an average plateout rate of 15 hr^{-1}. Since we are interested in the effects of particle removal on radon progeny concentrations, we have combined this average plateout rate with our estimate for the deposition rate of attached progeny to produce an overall removal rate as a function of particle concentration. The results of these calculations are presented

in Figure 26.

Discussion

As can be seen from the results of our radon progeny measurements, as shown in Tables 6 and 8, and Figures 24, 25, and 26, particle concentration is an important factor in assessing the effects of air cleaning on radon progeny concentrations. Thus we have combined the data from tests of the various control devices and present the results in terms of particle concentration rather than showing the effects of each individual air cleaner.

At particle concentrations between 3000 and 30000 particles/cm^3, which is the range typical of indoor concentrations, there are substantial amounts of free radon progeny, as can be seen from Figure 25. This is also a region of rapid change in the magnitude of the free fractions, where the unattached fractions range from 50 percent for ^{218}Po, 10 percent for ^{214}Pb, and 3 percent for ^{214}Bi at 3000 particles/cm^3 to 10 percent, 1 percent and 0.1 percent respectively at 30000 particles/cm^3.

As shown in Figure 26, the removal rate is a product of the free fraction and the plateout rate. Thus, the large free fractions at low particle concentration have an important effect on the overall progeny removal rate. As can be seen in Figure 26, the removal rate due to plateout and deposition is substantial over a large range of particle concentrations, although as shown in the inset, deposition is a significant fraction of the removal rate only for attached ^{214}Pb and ^{214}Bi at high particle concentrations. In comparison with removal rates for the control devices, plateout is the largest removal process for all three of the radon progeny species at particle concentrations below a few hundred particles/cm^3. For ^{218}Po, plateout continues to be a dominant removal process even at particle concentrations above 10000 particles/cm^3, while deposition, on the other hand, is not an important removal process at particle concentrations up to 100,000/cm^3.

Another means of gauging the effects of particle removal on radon progeny concentrations is the ratio of the Potential Alpha Energy Concentration (working level) to the radon concentration -- the working level ratio (WLR). We show in Figure 24, along with our measured working level ratios, calculated values for WLR indicated by the solid line. These calculations are based on our measured and derived values for the removal rates and unattached fractions for radon progeny, using Equation (26). The solid line in Figure 24 represents the calculated WLR assuming that the control device removal rate is zero. As can be seen in Figure 24, there are three distinct regions: for particle concentrations above $7000/cm^3$, the WLR is >0.60; for concentrations below $500/cm^3$, WLR is <0.08; between these two regions, the WLR changes quite rapidly through a range of particle concentrations typical of indoor environments. The calculated WLR values agree reasonably well with the measured values throughout the range in particle concentrations.

VI SUMMARY AND CONCLUSIONS

In this section, we first present a summary discussion of our tests
of unducted particulate control devices, reviewing the performance of
the devices themselves, and the effects of particulate control on radon
progeny concentrations. We then construct a hypothetical example to
illustrate the application of these results to a residential dwelling.

The performance tests of the air cleaners show a substantial varia-
tion in the abilities of various <u>classes</u> of devices to remove particles
from indoor air. Based on our results, simple panel-filter devices are
not effective in removing particles generated by tobacco combustion.
While these types of air cleaners appear to have a large share of the
consumer air cleaner market, our tests indicate they provide essentially
no air cleaning. We tested the effects of additional air circulation,
and found that it does not provide any measurable reduction in particu-
late concentrations, although we observed that additional air circula-
tion helps dissipate the visible smoke plume. Our results for the two
negative ion generators are mixed, and as we have discussed, the
residential unit which had both an emitter and collector surface does
not remove particles unless there is substantial air circulation. Even
then, the removal rate is still very modest. For the commercial ionizer
which had a higher negative voltage on the emitter and no integral col-
lector surface, the overall performance is better, although since room
walls, tables, etc. become the particle collection surfaces, soiling of
these surfaces may be a concern. The electrostatic precipitators and
extended surface filters we tested produced a significant reduction in
particle concentrations. However, we should emphasize that our tests
measured only the effectiveness with which the particulate phase contam-
inants of tobacco smoke were removed and should not be construed as evi-
dence for removal of the many gas phase contaminants, some of which are
best controlled by ventilation (e.g. carbon monoxide).

With regard to the effects of particulate control on radon progeny
concentrations two points emerge from these experiments. First, at low
to moderate particle concentrations, plateout is the single, most impor-
tant removal term. Thus, operation of an effective particulate-control

device contributes to radon progeny removal not only by filtration of attached and unattached radon decay products, but also by producing low particle concentrations so that plateout of unattached progeny is an important removal mechanism. As an illustration, the device we tested with the highest particle removal rate, the HEPA-type filter unit, has a removal rate of ~8 hr^{-1} and yielded concentrations of less than 100 particles/cm^3, where the corresponding progeny plateout rates are ~12 to 15 hr^{-1}. Second, even at moderate to high particle concentrations, the amount of <u>unattached</u> ^{218}Po is not negligible and removal of this nuclide by plateout is an important effect. Even at particle concentrations of 20000 to 50000, for example, this removal term is between 1 and 2 hr^{-1}, which, is greater than typical ventilation rates.

To illustrate further the results of these experiments, we have calculated equilibrium concentration values for particles and radon progeny in a house under several different ventilation and air cleaning scenarios. These are simplified hypothetical examples and application to a specific residence will require a more detailed treatment of indoor source and removal terms.

In each case we assume a 340 m^3 structure. Case A assumes an initial air change (ventilation) rate of 0.65 hr^{-1} and no additional <u>in-situ</u> air cleaning. For case B, we assume that the change rate is 0.5 hr^{-1}, a reduction from case A that might be achieved by weatherization and house-tightening; again no air cleaning is assumed. We note that the ventilation rate of 0.65 hr^{-1} for the unweatherized house and a 23 percent reduction in infiltration rate due to weatherization is based on average infiltration rates and weatherization effects (Turiel, et. al., 1983).

In the third and fourth cases for our hypothetical example, particulate control devices capable of providing effective clean air flows equivalent to 0.5 air change per hour for case C and 1.0 air change per hour for case D, are used to compensate for the reduction in ventilation. These effective clean air flows, 100 and 200 cfm respectively, could be obtained with some of the devices we tested. These cases are summarized in Table 9, along with our assumptions for the various

pollutant sources.

We assume a radon entry rate of 0.66 pCi/l hr^{-1}, which gives an equilibrium radon concentration of 1 pCi/liter for case A with a ventilation rate of 0.65 air change per hour. This assumption not only provides a convenient, easily-multiplied value for the indoor radon concentration (since the calculated PAEC values scale directly with radon concentration), it is also near the median of the range of radon entry rates determined for a sample of U.S. housing (Nero and Nazaroff, 1983c). Using the mass balance model for indoor particles we showed earlier in Equation (1), we can estimate the steady-state concentrations of particles for the four ventilation and/or control device assumptions and five indoor source terms. We have used as indoor particle sources tobacco combustion at the rate of 0, 0.5, 1, 2, and 4 cigarettes per hour and a small constant source term that might correspond to generation of particles from general occupant activity. In addition, we have assumed some penetration into the indoor environment of outdoor aerosols.

Based on the resulting particle concentrations for each scenario, we use Figure 25 to estimate the fraction of progeny that are unattached. Using Equation (26) the working level ratio (WLR) is computed for each case, which, when multiplied by the radon concentration gives the corresponding PAEC. We also estimate the PAEC due only to unattached progeny.

Several points of interest emerge from comparison of the results in Table 9. Tightening the house with no additional particulate control produces higher average particle concentrations for all cigarette smoking rates, except for a smoking rate of zero, where reduction in infiltration reduces the particle concentration, due to reduction in infiltrating outdoor particles. Use of an air cleaning device more than compensates for the reduced ventilation in terms of particle concentrations for all smoking rates. It is not clear that one could achieve the 3000 particles/cm^3 shown for case D, no smoking, in an actual situation since other sources that can be neglected when average particle concentrations are high will be more significant when the average particle load is low.

In the case of radon progeny the results are less straightforward. The radon progeny concentrations increase as one goes from case A to B. With the use of a moderate amount of particulate removal, as in case C, the PAEC drops compared to case B to values equivalent to those calculated for case A. Note that at higher smoking rates, the PAEC for case C does not drop quite as much as for the two lowest smoking rates. When an additional increment of particulate removal is added, case D, the PAEC drops again to values consistently below those found in case A.

Although no indoor radon progeny concentration standards have been established in this country for typical residences, we can compare our calculated values with guidelines recommended for use in the remedial action programs for clean-up of uranium mill tailings. These are (PHS 1972):

>0.05 WL   Remedial action indicated

0.01 - 0.05 WL Remedial action may be suggested

<0.01 WL   No action indicated

The American Society of Heating, Refrigeration, and Air Conditioning Engineers (ASHRAE) has recommended a guideline of 0.01 WL (ASHRAE, 1981). At an initial radon concentration of 1.0 pCi/l, none of the resulting PAEC values in our hypothetical example exceed 0.01 WL (10 mWL). For a radon concentration of 4 pCi/l, near the upper end of the range of concentrations commonly found in U.S. housing (Nero and Nazaroff, 1983c), progeny concentrations for only case D at a zero smoking rate would fall below 0.01 WL (10 mWL). At the opposite extreme, our estimates indicate that under circumstances where the radon concentration is higher than average, e.g. 10 - 15 pCi/l, and indoor particulate concentrations are equivalent to that produced by a smoking rate of greater than 1 cigarette per hour, the remedial action guideline of 0.05 WL would be approached or exceeded, even with substantial particulate control, as in case D.

As we discussed earlier in this paper, lung dosimetry models predict a higher lung dose from unattached radon progeny that are inhaled then deposited in the lung. Thus, an estimate of the PAEC due to these unattached decay products would provide a _relative_ basis for comparing the effects of particulate control. For the PAEC due to the unattached progeny, the case A values are the lowest for all smoking rates. Even when a large amount of air cleaning is used, as in case D, these PAEC values do not drop to levels calculated for case A, although case D does have $PAEC_{free}$ values lower than for case C, which in turn is lower than case B.

As our simplified set of scenarios illustrate, the use of air cleaning can compensate for the higher particulate levels that may result from reduced ventilation rates. On the other hand, for those situations where indoor radon levels are of concern, reduction of radon progeny concentrations will require a more substantial air cleaning effort than is needed for control of particulate concentrations only. In the case of exposure to unattached progeny, the increase in the PAEC due to reduced ventilation is not fully compensated by the use of particulate removal devices.

Additional Research

This work is an evaluation of air cleaning devices under a limited set of conditions. Research using other sources of particles, such as combustion of natural gas and kerosene or possibly non-combustion aerosols, would extend the testing of air cleaning devices to other common indoor particles with different physical and chemical properties than aerosols from tobacco smoke. Additional studies with different operating conditions, such as tests conducted at high relative humidities (above 60 percent) would be helpful in further characterizing the performance of electrostatic devices and ionizers. Further study of the interaction of radon progeny and indoor aerosols will provide a better understanding of the effects of air cleaning on radon progeny concentrations. Direct measurement of the free progeny concentrations would help verify the results presented in this work.

ACKNOWLEDGEMENTS

VII.REFERENCES

ACHR, Air Conditioning, Heating, and Refrigeration News, May 3, 1982.

ASHRAE, 1976, "Std 52-76 Method of Testing Air-Cleaning Devices Used for Removing Particulate Matter," American Society of Heating, Refrigeration, and Air Conditioning Engineers, New York, NY.

ASHRAE, 1981, "Standard 62-81 Ventilation for Acceptable Indoor Air Quality", American Society of Heating, Refrigeration, and Air Conditioning Engineers, Atlanta, GA.

Bowker, A.H., and Lieberman, G.J., 1972, Engineering Statistics 9, 336-338, Prentice-Hall, Inc., Englewood Cliffs, NJ.

Bruno, R.C., 1983, "Verifying a Model of Radon Decay Product Behavior Indoors," Health Physics, 45, 471-480.

Busigin, A., A.W. van der Vooren, J.C. Babcock and C.R. Phillips, 1981, "The Nature of Unattached RaA (^{218}Po) Particles," Health Physics, 40, 333-343.

Harley, N.H., and B.D. Pasternak, 1981, "A Model for Predicting Lung Cancer Risks Induced by Environmental Levels of Radon Daughters," Health Physics, 40, 307-316.

Hinds, W.C., 1978, "Size Characteristics of Cigarette Smoke," Am. Ind. Hyg. J., 39, 48-54.

Institute of Environmental Sciences, 1968, "Standard for HEPA Filters," IES-CS-1, Mt. Prospect, IL.

Jacobi, W., 1972, "Activity and Potential Alpha-Energy of ^{222}Rn and ^{220}Rn Daughters in Different Air Atmospheres," Health Physics, 22, 441+.

Jacobi, W, and K. Eisfeld, 1980, "Dose to Tissues and Effective Dose Equivalent by Inhalation of ^{222}Rn, ^{220}Rn and Their Short-lived Daughters," GSF Report S-626.

James, A.C., W. Jacobi, and F. Steinhausler, 1981, "Respiratory Tract Dosimetry of Radon and Thoron Daughters: The State-of-the-Art and Implications for Epidemiology and Radiobiology," in <u>Radiation Hazards in Mining</u>: <u>Control, Measurement, and Medical Aspects</u>, ed. by M. Gomez, (New York: Society of Mining Engineers).

Knutson, E.O., A.C. George, J.J. Frey, and B.R. Koh, 1983, "Radon Daughter Plateout - II, Prediction Model," <u>Health Physics</u>, <u>45</u>, 445-452.

Malstrom, T.G., and A. Ahlgren, 1981, "Aspects of Efficient Ventilation in Office Rooms," Royal Institute of Technology, Division of Heating and Ventilating, Stockholm, Sweden.

Melandri, C., G. Tarrani, V. Prodi, T. De Zaiacomo, M. Formignani, and C.C. Lombardi, 1983, "Deposition of Charged Particles in the Human Airways," <u>J. Aerosol Sci.</u>, <u>14</u>, 184-186.

Mercer, T.T., 1976, "The Effect of Particle Size on the Escape of Recoiling RaB Atoms from Particulate Surfaces," <u>Health Physics</u>, <u>31</u>, 173+.

Nazaroff, W.W., 1980, "A Residential Radon Daughter Monitor Based on Alpha Spectroscopy", Lawrence Berkeley Laboratory Report LBL-10768.

Nazaroff, W.W., M.L. Boegel, and A.V. Nero, 1981a, "Measuring Radon Source Magnitude in Residential Buildings," Lawrence Berkeley Laboratory Report LBL-12484.

Nazaroff, W.W., K.L. Revzan and A.W. Robb, 1981b, "Instrumentation for a Radon Research House," Lawrence Berkeley Laboratory Report LBL-12564.

Nazaroff, W.W. 1983a, "Radon Daughter Carousel: An Automated Instrument for Measuring Indoor Concentrations of ^{218}Po, ^{214}Pb, and ^{214}Bi," <u>Review of Scientific Instruments</u>, <u>54</u>, 1227-1233.

Nazaroff, W.W., H Fuestel, A.V. Nero, K.L. Revzan, D.T. Grimsrud, M.A. Essling, and R.E. Toohey, 1983b, "Radon Transport into a Single-Family House with a Basement," Lawrence Berkelely Laboratory Report LBL-16572.

Nero, A.V., 1983a, "Indoor Radiation Exposures from ^{222}Rn and Its Daughters: A View of the Issue," Health Physics, 45, 277-288.

Nero, A.V., 1983b, "Airborne Radionuclides and Radiation in Buildings: A Review" Health Physics, 45, 303-322.

Nero, A.V., and W.W. Nazaroff, 1983c, "Characterizing the Source of Radon Indoors," Lawrence Berkeley Laboratory Report LBL-16636, Presented at the International Seminar on Indoor Exposure to Natural Radiation and Related Risk Assessment, Capri, Italy, 1983.

New Shelter, 1982, "A test of Small Air Cleaners," Rodale's New Shelter, Rodale Press.

Offermann, F.J., Fisk, W.J., Grimsrud, D.T., Pedersen, B., and Revzan, K.L., 1983, "Ventilation Efficiencies of Wall- or Window-mounted Residential Air-to-air Heat Exchangers," ASHRAE Transactions, 1983.

Otto, R.J., private communication, 1983.

Picot, A., 1980, "Pocket Calculator Program for Least-square Fitting of Data with Variable Precision," Am. J. Phys., 48 (4)

Porstendoerfer, J.W., A. Wicke, and A. Schraub, 1978a, "The Influence of Exhalation, Ventilation and Deposition Processes upon the Concentration of Radon and Thoron and Their Decay Products in Room Air," Health Physics, 34, 465+.

Porstendoerfer, J.W., and T.T. Mercer, 1978b, "Influence of Nuclei Concentration and Humidity Upon the Attachment Rate of Atoms In the Atmosphere," Atmospheric Environment, 12, 2223-2228.

Public Health Service, 1972, 'Grand Junction Remedial Action Criteria,' U.S. Department of Health, Education, and Welfare, Federal Register, 37, 25918-9, (37 FR 25918).

Sandberg, M., 1981, "What is Ventilation Efficiency?", Building and Environment, 16, 123-135.

A.G. Scott, 1983, "Radon Daughter Deposition Velocities Estimated From Field Measurements," Health Physics, 45, 481-485.

Task Group on Lung Dynamics, 1966, "Deposition and Retention Models for Internal Dosimetry of the Human Respiratory Tract," Health Physics, 12, 173-207.

Thomas, J.W., and R.J. Countess, 1979, "Continuous Radon Monitor, Health Physics, 36, 734-738.

Turiel, I., W.J. Fisk, and M. Seedall, 1983, "Energy Savings and Cost-Effectiveness of Heat Exchanger Use as an Indoor Air Quality Mitigation Measure in the BPA Weatherization Program," Energy, 8, 323-335.

UNSCEAR, 1982, Ionizing Radiation: Sources and Biological Effects, United Nations Scientific Committee on the Effects of Atomic Radiation, United Nations, New York, 173.

Whitby, K.T., Anderson, G.R., and Rubow, K.L., 1983, "Dynamic Method for Evaluating Room Size Air Purifiers," ASHRAE Transactions, 1983.

Wicke, A. and J. Porstendoerfer, 1982, "Radon Daughter Equilibrium in Dwellings," in Natural Radiation Environment, ed. by K.G. Vohra, et. al., Wiley Eastern Ltd., New Dehli, 481-488.

TABLE CAPTIONS

Table 1.   Sources of Indoor Suspended Particulate Matter

Table 2.   Airflow Rates and Power Consumption of Portable Air Cleaners

Table 3.   Summary of Test Procedure

Table 4.   Portable Air Cleaner Descriptions and Results

Table 5.   Comparison of Air Cleaner Performance Measurements Made by Different Laboratories

Table 6.   Total Radon Progeny Removal Rates and Working Level Ratios for Different Particle Concentrations

Table 7.   Values of Measured and Derived Decay Parameters

Table 8.   Unattached Fraction for Radon Progeny Estimated as a Function of Particle Concentration

Table 9.   Predicted Concentrations of Respirable Particles and Radon Progeny Working Levels for a Hypothetical Residence

Table 1.
Sources of Indoor Suspended Particulate Matter

INDOOR SOURCES

Building Materials

Insulation

- fiberglass fibers

- cellulose fibers

Fire retardant

- asbestos fibers

Building Contents

Combustion devices

- unvented gas range emissions

- unvented kerosene and gas heater emissions

- wood stove and fireplace emissions

Occupants

- bacteria, scales, viruses

Occupant activities

- tobacco smoke

- aerosol sprays

- cooking emissions

- resuspended household dust

INFILTRATING OUTDOOR SOURCES

- plant pollen and spores

- atmospheric dust

- combustion emissions from mobile and stationary sources

Table 2.
Airflow Rates and Power Consumption of Portable Air Cleaners

Device type	Manufacturer Model	Speed	Power (watts)	Airflow Rate (cfm)	Ratio (cfm/watt)
Thin Panel Filters	Rush Hampton 7305	high	20	10	0.5
		low	15	7	0.5
	Norelco HB1920	high	27	29	1.1
		low	16	18	1.1
	Pollenex 699	high	18	21	1.2
		low	10	12	1.2
	Neolife Consolaire	high	40	29	0.7
		medium	28	17	0.6
		low	22	13	0.6
Extended Surface Filters	Bionaire 1000	high	32	66	2.1
		medium	23	59	2.6
		low	7	29	1.7
	Summitt Hill Hepanaire HP-50	high	98	202	2.1
		medium	67	157	2.3
		low	52	102	2.0
Electrostatic Filters	Trion Console	high	*	*	*
		medium	109	215	2.0
		low	77	146	1.9
	Summitt Hill Micronaire P-500	high	122	255	2.1
		medium	77	200	2.6
		low	54	120	2.2

* air flow rate above current capability of test equipment

Table 3
Summary of Test Procedure

Duration (hrs)	Activity
0.1	Initial particle and radon injection
4	Natural mixing and decay
3 - 5	Control device operation
6 - 8	Natural decay (or growth) period
~8	Room ventilation and dehumidification in preparation for the next test

Table 4.   Portable Air Cleaner Descriptions and Results

Device type	Manufacturer Model	Device description	Retail costs ($)[a] device	Retail costs ($)[a] filter	Speed	Power (watts)	Flowrate (cfm)	Efficiency[b] (%)	ECR[c] (cfm)
Panel Filters	Rush Hampton 7305	foam filter	30	4	high	20	10	0±1	0±1
	Norelco HB 1920	electret filter	40	5	high	27	29	11±1	3±1
	Pollenex 699	electret filter	35	6	high	18	21	16±3	3±1
	Neolife Consolaire	negative corona charging and electret filter	150	12	med.	28	17	39±11	7±2
Extended Surface Filters	Bionaire 1000	electret filter and negative ion-generator	300	16	high	32	66	86±9	57±2
	Summit Hill Hepanaire HP-50	HEPA filter	395	77	med.	67	157	115±13	180±8
Electrostat Precipitators	Trion Console	two-stage flat plate positive corona	370	15 (carbon)	med.	109	215	57±11	122±19
	Summit Hill Micronaire P-500	two-stage flat plate positive corona	395	15 (carbon)	med.	77	200	58±6	116±5
Ion-Generators	ISI Orbit	residential model negative corona positive collector	80	none	--	2	0	--	1±1
	Zestron Z-1500	commercial model negative corona no collector	120	none	--	3	0	--	30±1
Circulating Fan	Dayton 4C507	oscillating fan 2 units	52 each	none	high	44 each	1800 each	0±1	0±1

a. Retail costs obtained from manufacturers or local distributors (prices as of mid-1983).

b. Efficiency calculated as the observed effective cleaning rate (ECR divided by the measured air flow rate (± 90% confidence limits). See note below for ECR definition.

c. Effective cleaning rate (ECR) calculated as the flow rate of particulate free air required to produce the observed decay rate in cigarette smoke (± 90% confidence limits).

Table 5. Comparison of air cleaner performance measurements made by different laboratories.

Air Cleaner Type	Manufacturer	Model	Effective Cleaning Rates [cfm (±)] [a]		
			LBL	Lab A[b]	Lab B[c]
Panel Filters:	Neo-Life Company of America	Neolife Consolaire	7 (2)	-	-
	Norelco/North Amer. Corp.	Norelco Clean Air Machine II HB1920	3 (2)	2	-
	Associated Mills Inc.	Pollenex Pure Air 99 Model 699	3 (0)	0	-
	Pyramid Products	Nature Fresh AP 30-B1	-	0	-
	Remington Products Inc.	Remington Air Purifier AP-100	-	0	-
	Rival Manufacturing Co.	Rival Air Cleaner 2800	-	0	-
	Ronco Inc.	Clean Aire 1917	-	2	-
	Rush Hampton Ind. Inc.	Ecologizer Air Treatment System 3305	-	0	-
	Rush Hampton Ind. Inc.	Ecologizer Air Treatment System 7305	0 (0)	-	-
	Shetland Co.	Air Freshener 8001	-	0	-
	Sunbeam Appliance Co.	Fresh Aire 57-16	-	1	-
	Van Wyck Int'l Corp.	Country Fresh Air 360 03-2401	-	0	-
	Vaportex Inc.	Vaportex Air Purifier 90-0971	-	0	-
	Welco Mfg. & Trading Co.	Refresh-Aire RA-1	-	0	-
	Unknown		-	-	0 (0)

Extended Surface Filters:	Air Techniques Inc.	Cleanaire 1212	–	39	–
	Biotech Electronics Ltd.	Bionaire 1000	57 (2)	59	–
	Summit Hills Inc.	Hepanaire HP-50	180 (8)	–	–
Electrostatic Precipitators:	Trion Inc.	Console Model	122 (19)	–	–
	Summit Hill Inc.	Micranaire P-500	116 (5)	–	–
	Unknown		–	–	12 (1)
Ion-Generators:	The Amcor Group Ltd.	FreshenAire 301-243	–	16	–
	DEV Ind.	Air Care II Environmental System	–	5	–
	Ion Research Center	Ion Fountain	–	44	–
	Ion Systems Inc.	Ionosphere	–	38	–
	Ion Systems Inc.	Orbit	1 (0)	17	–
	Zestron Inc.	Z-1500	30 (1)	–	–
Air Circulators:	3420 Dayton Electric Mfg. Co.	Dayton Portable Circulator Fan 4C418	–	2	–
	3600 Dayton Electric Mfg. Co.	2 Dayton Table Mounted Oscillating Circulators 4C507	0 (1)	–	–

a) Effective cleaning rate is calculated as the flow rate of particulate free air required to produce the observed decay rate of cigarette smoke.

b) Calculated from tests published by NEW SHELTER July/August 1982.

c) As reported by Whitby et.al., "Dynamic Method for Evaluating Room-Size Air Purifiers," ASHRAE Transactions 1983.

Table 6

Total Radon Progeny Removal Rates and
Working Level Ratios for Different Particle Concentrations

Particulate Concentration (particles/cm^3)	Removal Rate (hr^{-1})			Working Level Ratio
	Λ_1	Λ_2	Λ_3	
Before device operation				
35000	1.62	.084	.101	.81
30000	1.18	.079	.074	.86
28000	2.05	.105	.046	.811
31000	1.01	.084	.074	.875
24000	2.26	.058	.083	.815
38000	.96	.105	.108	.866
2800	7.74	1.0	.273	.392
30000	1.54	.131	-.02	.833
14000	2.10	.11	-.05	.814
9000	2.71	.11	-.02	.79
33000	2.00	.063	.145	.807
31000	1.04	.048	.058	.881
60000	0.73	.051	-.067	.919
End of device operation				
45	21.9	17.7	10.3	.058(*)
⁻500	18.3	16.5	9.5	.067(*)
120	23.0	8.5	2.9	.076(*)
13000	3.10	.11	-.01	.764
230	19.5	12.7	1.26	.076
7800	3.75	.286	.153	.650
90	21.7	11.9	2.78	.071
15000	6.09	.28	.027	.584
60	14.4	7.73	3.88	.103

* Λ_i and WLR based on grab sample measurements

Table 7
Values of Measured and Derived
Decay Parameters

Parameter	Value or Functional Form	Reference	Note:
Ventilation rate, λ_v	0.05 hr^{-1}	this work	1
Deposition rate, $\lambda_d{}^a$	0.16 hr^{-1} (count)	this work	3
Filtration rate, λ_F	variable (attached = free)	this work	2
Attachment rate, X	$= 4.3 \times 10^{-3}$ hr^{-1}x [particle concentration]	Porstendoerfer, et. al, 1978a	
Recoil probability, r	0.83	Mercer 1976	
Plateout rate, $\lambda_{po}{}^f$	15 hr^{-1}	this work	3

1. Average for most experiments. For those tests with measured rates higher than this, the higher values were used in the data analysis.

2. The filtration rate for attached progeny is the rate measured for aerosol removal. For unattached progeny, the filtration rate is assumed to be equivalent. See discussion in text.

3. See discussion in text.

Table 8

Unattached Fraction for Radon Progeny Estimated
as a Function of Particle Concentration

Particle Concentration (particles/cm^3)	Attachment Rate, X (hr^{-1})	Filtration Rate, λ_F (hr^{-1})	Unattached Fraction (percent)		
			f_1	f_2	f_3
Before device operation					
35000	151	–	8.4	0.95	0.05
30000	129	–	9.7	1.1	0.08
28000	120	–	10.3	1.2	0.11
31000	133	–	9.4	1.0	0.07
31000	133	–	9.4	1.0	0.09
24000	103	–	11.8	1.4	0.09
38000	163	–	7.8	0.87	0.04
2800	12	–	53.4	10.9	0.96
30000	129	–	9.7	1.1	0.15
14000	60	–	18.6	2.4	0.40
9000	39	–	26.3	3.7	0.66
33000	142	–	8.9	1.0	0.02
31000	133	–	9.4	1.1	0.08
60000	258	–	5.1	0.56	0.09
End of device operation					
45	0.19	8.3	99.2	97.8	95.7
500	2.15	6.3	90.4	76.0	55.5
120	0.52	2.5	96.9	88.0	78.9
13000	55.9	0.24	20.1	3.0	0.8
8100	34.8	0.05	28.4	4.2	0.5
230	0.99	3.9	94.7	83.1	78.2
7800	33.5	0.1	29.3	4.47	0.55
90	0.39	2.5	97.7	90.4	83.4
15000	64.5	0.0	17.6	2.2	0.25
60	0.26	1.6	98.4	92.0	82.1
17	0.07	8.3	99.7	99.2	98.9

Predicted Concentrations of Respirable Particles
and Radon Progeny Working Levels for a Hypothetical Residence

ASSUMPTIONS:

House volume = $340 \ m^3$

Outdoor aerosol concentration, C_o = 35 $\mu g/m^3$, = 20000 particles/cm^3

Penetration factor, outdoor to indoor transport, p = 0.5

Indoor particulate source strengths:

Cigarette combustion, S_{cig} = 32 mg/cig = 3.5×10^{12} particles/cig

Other sources = 0.63 mg/hr, = 6.3×10^9 partcles/hr

Particle deposition rate, $k_d = \lambda_d^a$ = 0.2 hr^{-1}

Unattached progeny plateout rate, λ_{po}^f = 15 hr^{-1}

Radon source strength, S_{Rn} = 0.65 pCi/liter-hr

RESULTS:

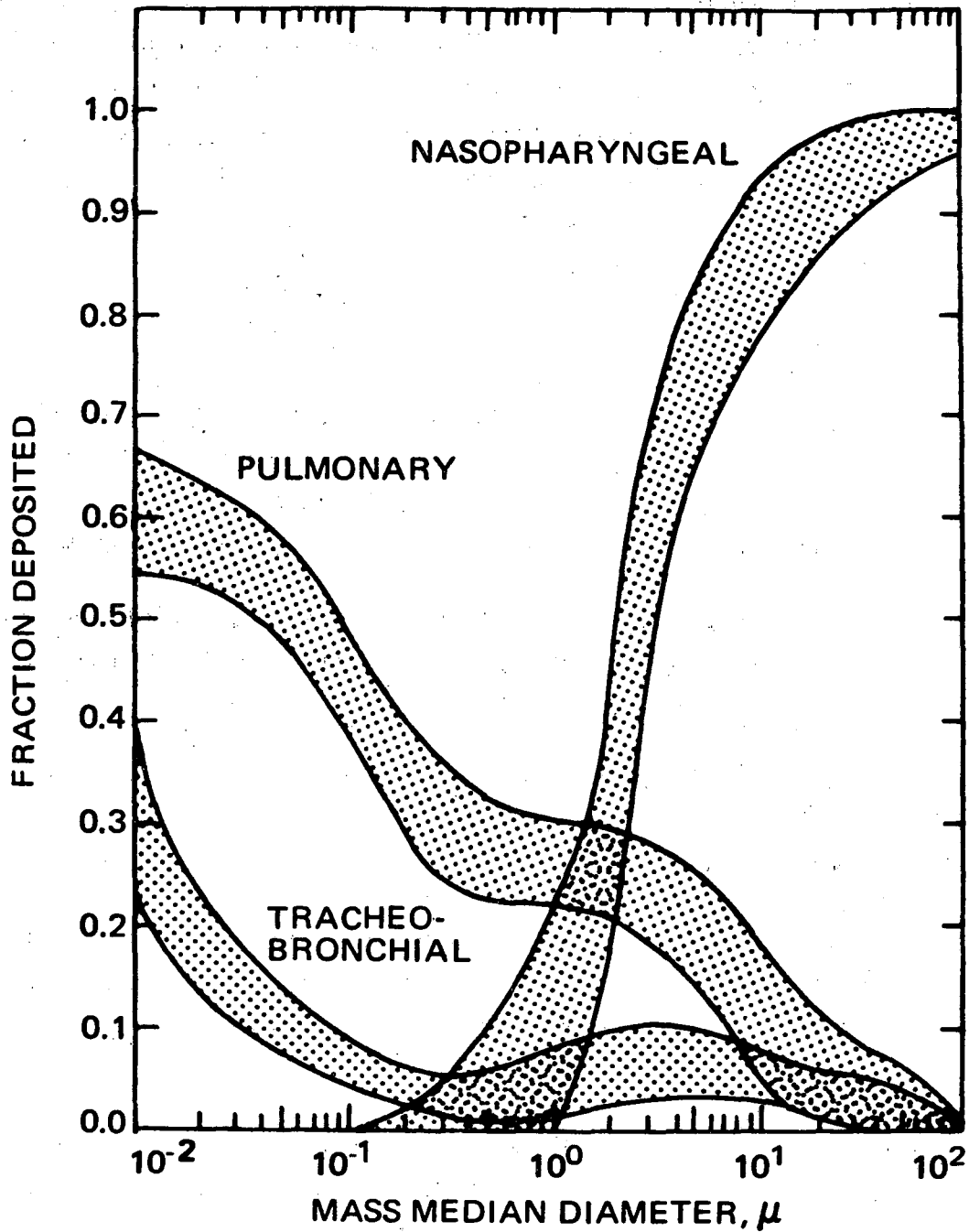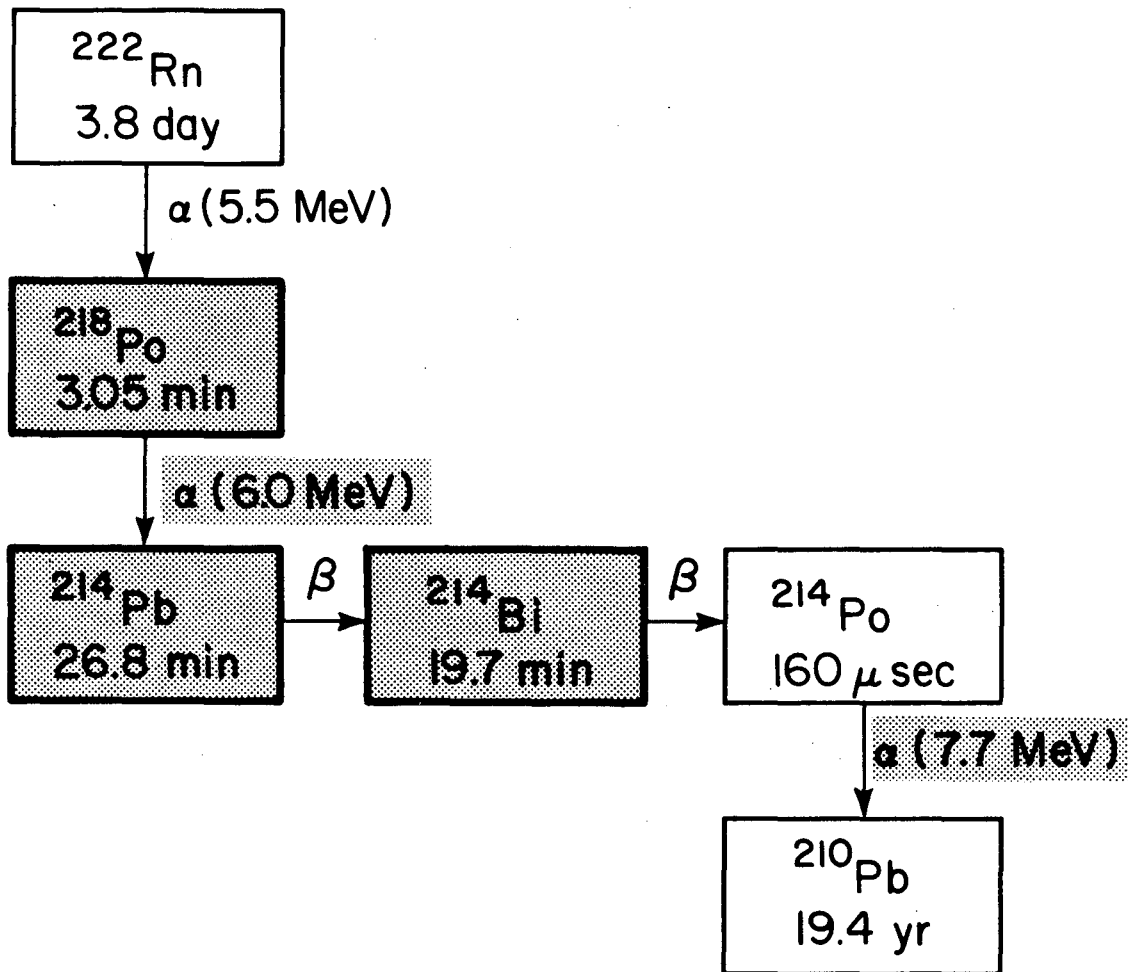|	Radon Conc. A_0 (pCi/l)	Ventilation Rate λ_V (1/hr)	Air Cleaning λ_F (1/hr)	Smoking Rate (cigarettes/hr)				
				0	0.5	1	2	4
CASE A:	1.0	0.65	0					
particle concentration								
(part/cm^3)				7700	13700	19800	31900	56100
($\mu g/m^3$)				16	71	126	237	458
WLR				0.361	0.426	0.460	0.498	0.529
PAEC (mWL*)				3.6	4.3	4.6	5.0	5.3
PAEC$_{free}$(mWL)				0.31	0.22	0.17	0.11	0.07
CASE B:	1.3	0.5	0					
particle concentration								
(part/cm^3)				7170	14500	21800	36600	65900
($\mu g/m^3$)				15	82	150	284	553
WLR				0.373	0.461	0.505	0.547	0.580
PAEC (mWL)				4.9	6.0	6.6	7.1	7.5
PAEC$_{free}$(mWL)				0.43	0.29	0.21	0.13	0.08
CASE C:	1.3	0.5	0.5					
particle concentration								
(part/cm^3)				4200	8500	12800	21300	38500
($\mu g/m^3$)				9	48	87	166	323
WLR				0.248	0.322	0.360	0.401	0.436
PAEC (mWL)				3.2	4.2	4.7	5.2	5.7
PAEC$_{free}$(mWL)				0.53	0.36	0.29	0.20	0.12
CASE D:	1.3	0.5	1.0					
particle concentration								
(part/cm^3)				3000	6000	9000	15100	27200
($\mu g/m^3$)				6	34	62	117	228
WLR				0.186	0.248	0.281	0.315	0.345
PAEC (mWL)				2.4	3.2	3.7	4.1	4.5
PAEC$_{free}$(mWL)				0.57	0.42	0.33	0.23	0.16

* 1 WL = 1000 mWL

FIGURE CAPTIONS

Figure 1.   Fraction of particles deposited in the three respiratory compartments as a function of particle diameter. (This figure shows the deposition efficiencies as calculated by the Task Group on Lung Dynamics)
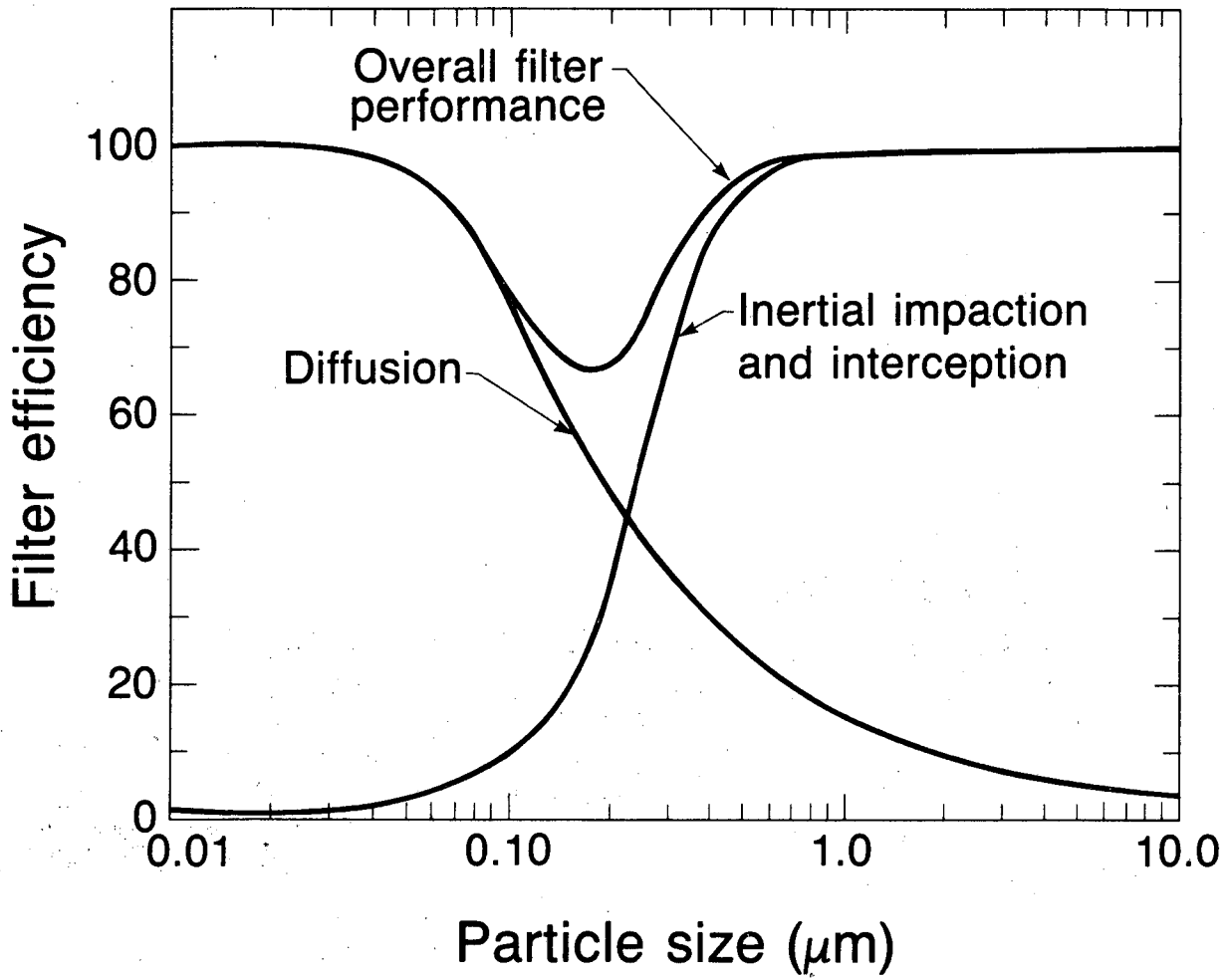
Figure 2.   Radon and radon progeny decay chain. The shaded isotopes are those of primary radiological concern due to inhalation and subsequent alpha decay (shaded). The shaded alpha decays are also those used to measure radon progeny concentrations.

Figure 3.   Particle removal efficiency as a function of particle size for a typical fibrous filter. (Adapted from Hinds, W.C., 1982, Aerosol Technology)

Figure 4.   Particle migration velocity as a function of particle size for a typical set of charging and electric field conditions. (Adapted from Oglesby and Nichols, 1977, Air Pollution, Third Edition, Arthur Stern, ed.)

Figure 5.   Schematic drawing of a two stage flat plate electrostatic precipitator

Figure 6.   Photograph of nine of the eleven portable air cleaners tested.

Figure 7.   Illustration of indoor contaminant mass balance model.

Figure 8.   Photograph of the Indoor Air Quality Research House (IAQRH) located at the University of California Richmond Field Station, Richmond, CA

Figure 9.   Floor plan of the Room 1 test space in the Indoor Air Quality Research House

Figure 1. Fraction of particles deposited in the three respiratory
compartments as a function of particle diameter. (This
figure shows the deposition efficiencies as calculated by
the Task Group on Lung Dynamics).

XBL 771-7190

RADON DECAY CHAIN

Figure 2.   Radon and radon progeny decay chain. The shaded isotopes
            are those of primary radiological concern due to inhalation
            and subsequent alpha decay (shaded). The shaded alpha
            decays are also those used to measure radon progeny concen-
            trations.

XBL 8310-3352

Figure 3. Particle removal efficiency as a function of particle size for a typical fibrous filter. (Adapted from Hinds, W.C., 1982, Aerosol Technology).
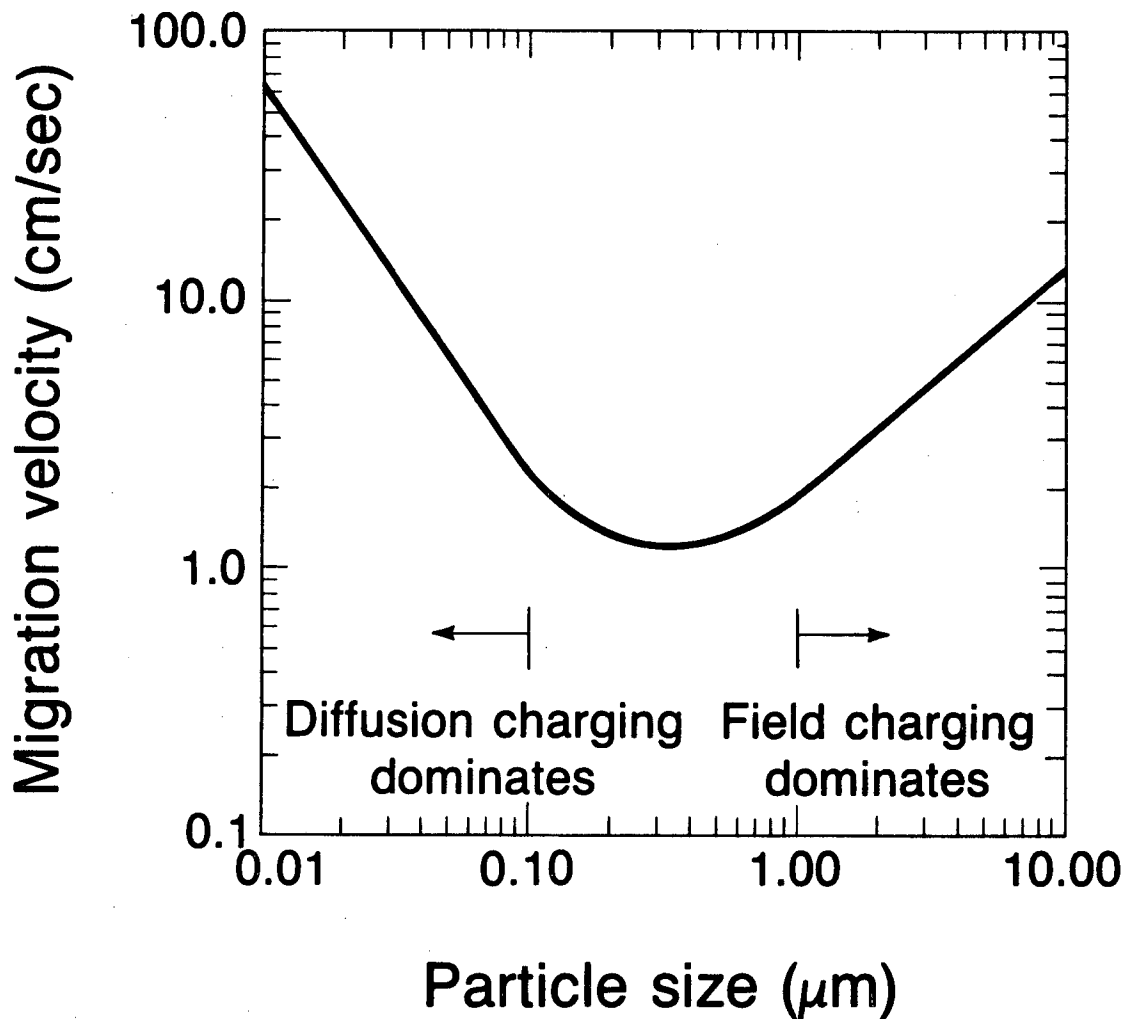
Figure 4. Particle migration velocity as a function of particle size
for a typical set of charging and electric field conditions.
(Adapted from Oglesby and Nichols, 1977, <u>Air</u> <u>Pollution</u>,
Third Edition, Arthur Stern, ed.)
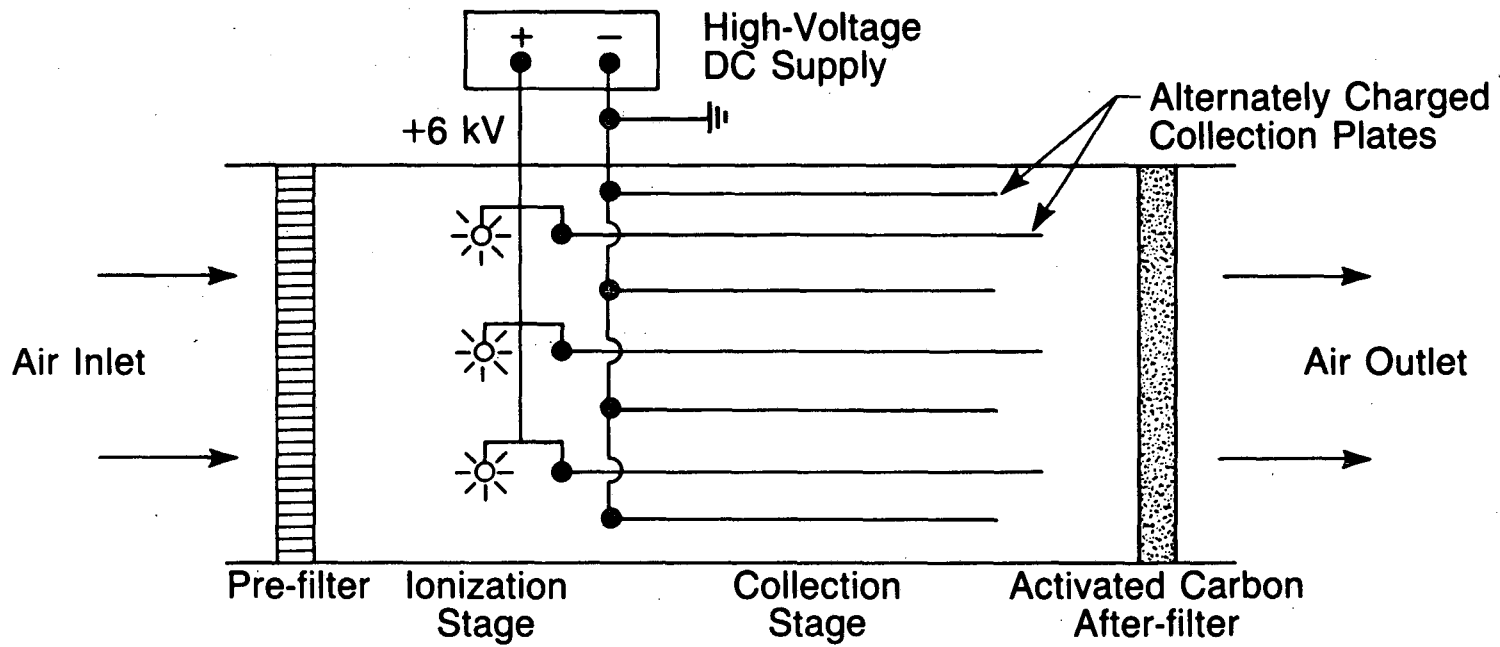
XBL 8310-3353

Figure 5.   Schematic drawing of a two stage flat plate electrostatic
precipitator.
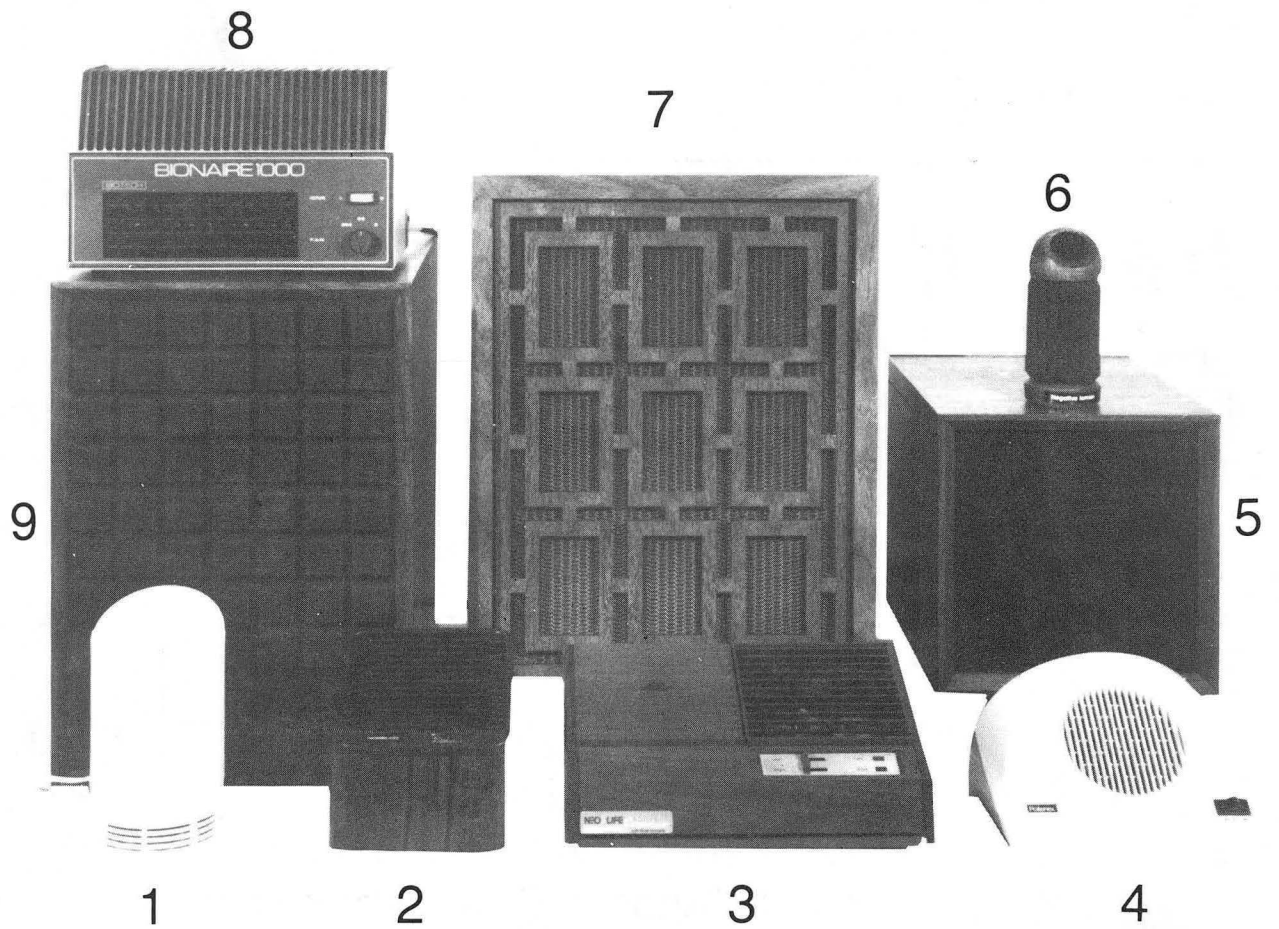
1. Rush Hampton 7305
2. Norelco-HB 1920
3. Neolife Consolaire
4. Pollenex 699
5. Summit Hill Micronaire
6. ISI Orbit
7. Trion Console
8. Bionaire 1000
9. Summit Hill Hepanaire

CBB 830-9619A

Figure 6.   Photograph of nine of the eleven portable air
cleaners tested.

$$PQ_IC_O \rightarrow$$

$$kC_i$$

$$Q_DC_i$$

Air Cleaner

$$Q_DC_i(1-\eta)$$

$$Q_IC_i \rightarrow$$

$$S$$
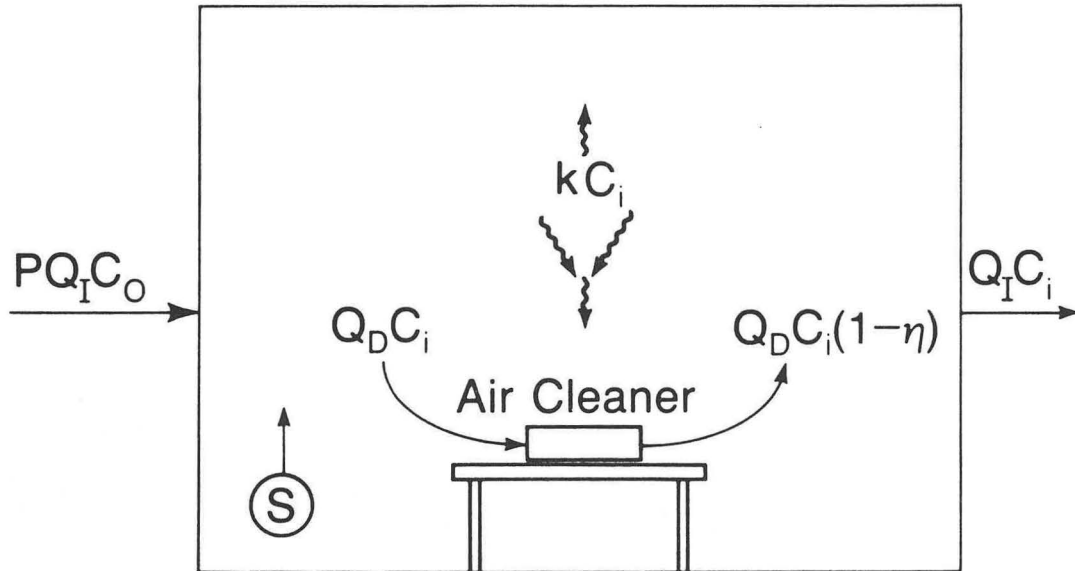
P = Penetration Factor
Q_I = Infiltration Airflow Rate
C_O = Outdoor Concentration
S = Indoor Source
Q_D = Air Cleaner Airflow Rate
η = Air Cleaner Efficiency
k = Contaminant Reactivity
C_i = Indoor Concentration

XBL 8310-3340

Figure 7.   Illustration of indoor contaminant mass balance model.
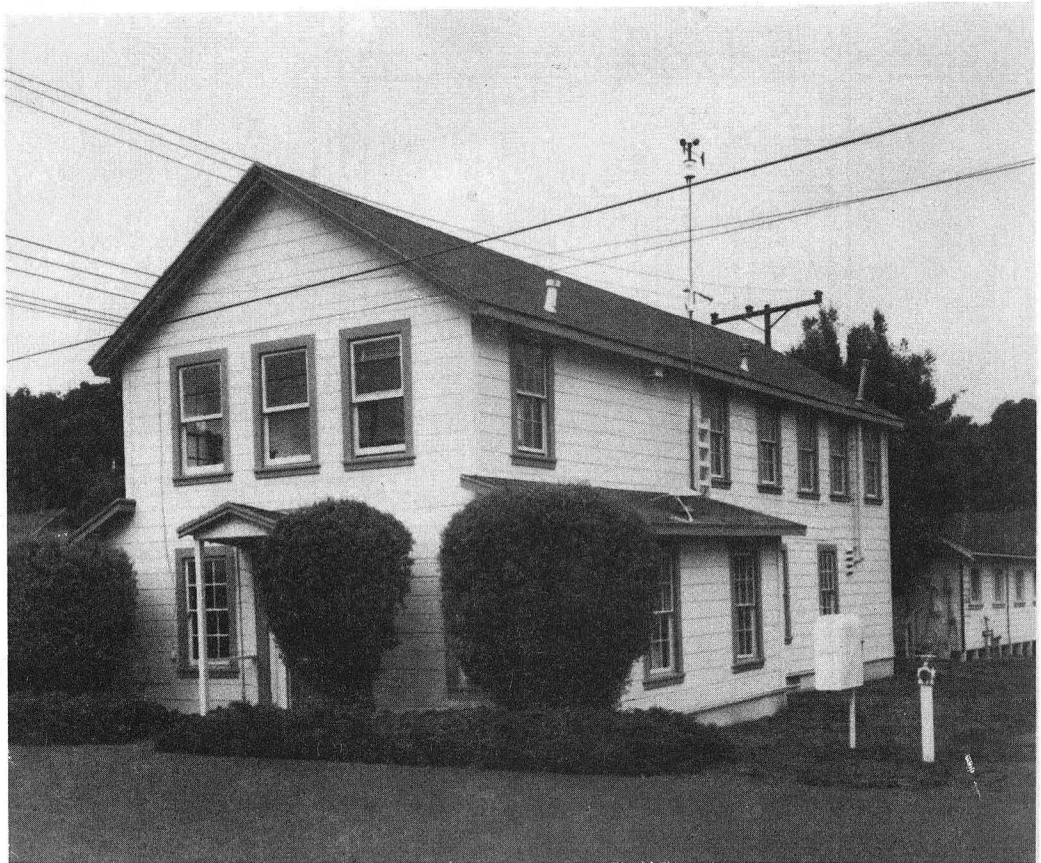
CBB 830-9631

Figure 8.   Photograph of the Indoor Air Quality Research House (IAQRH)
            located at the University of California Richmond Field Sta-
            tion, Richmond, CA
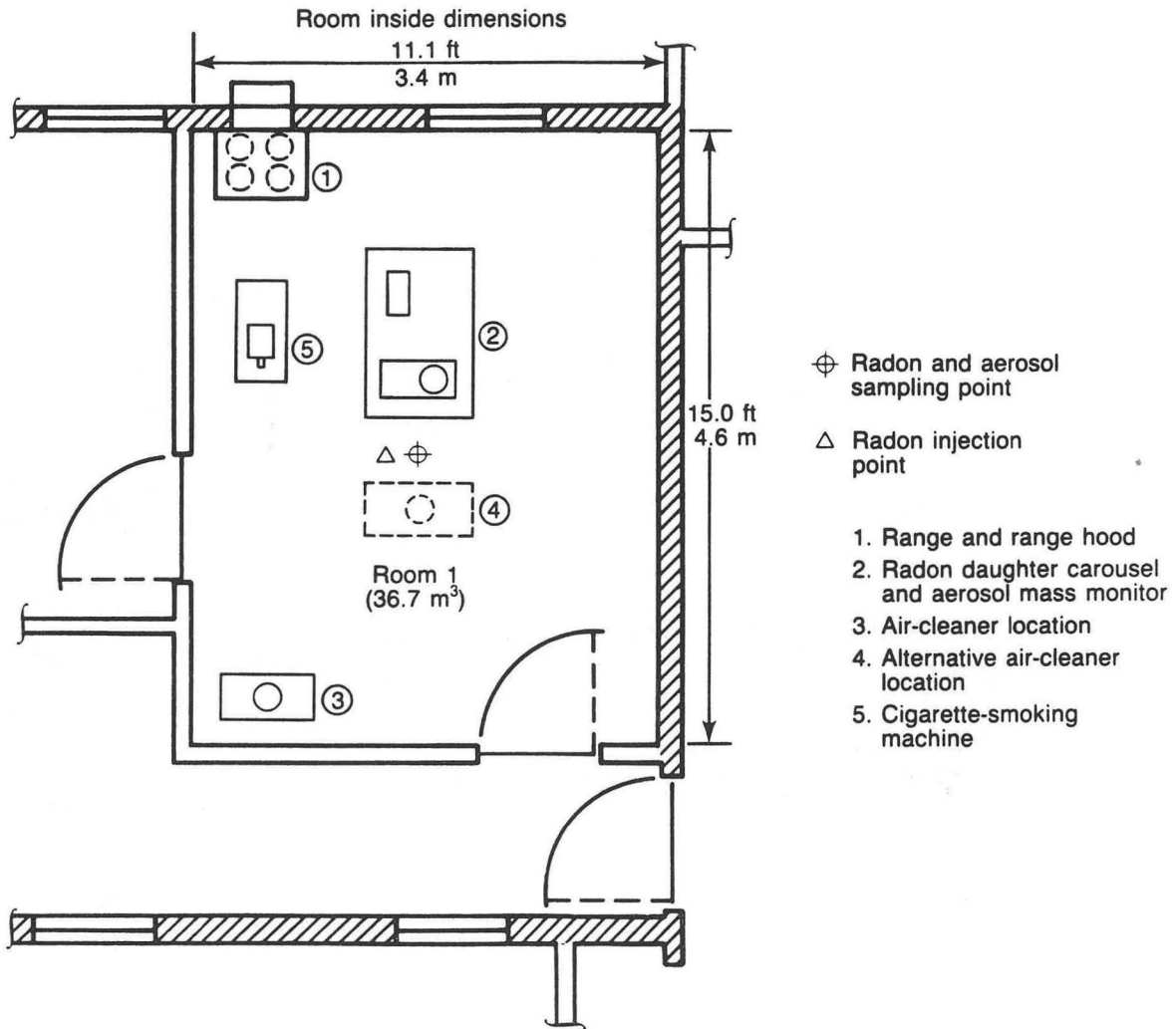
Figure 9.   Floor plan of the Room 1 test space in the Indoor Air
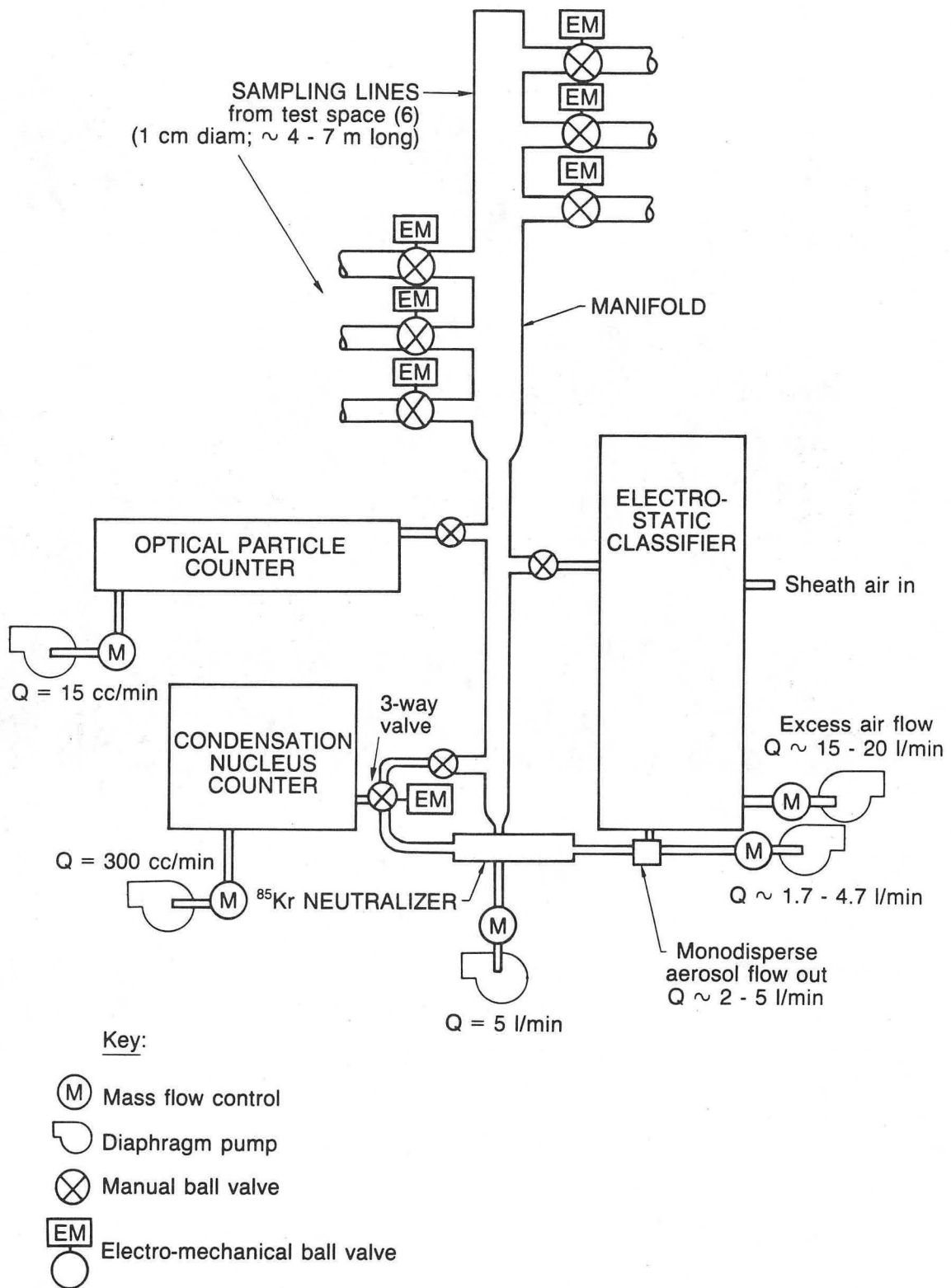Quality Research House.
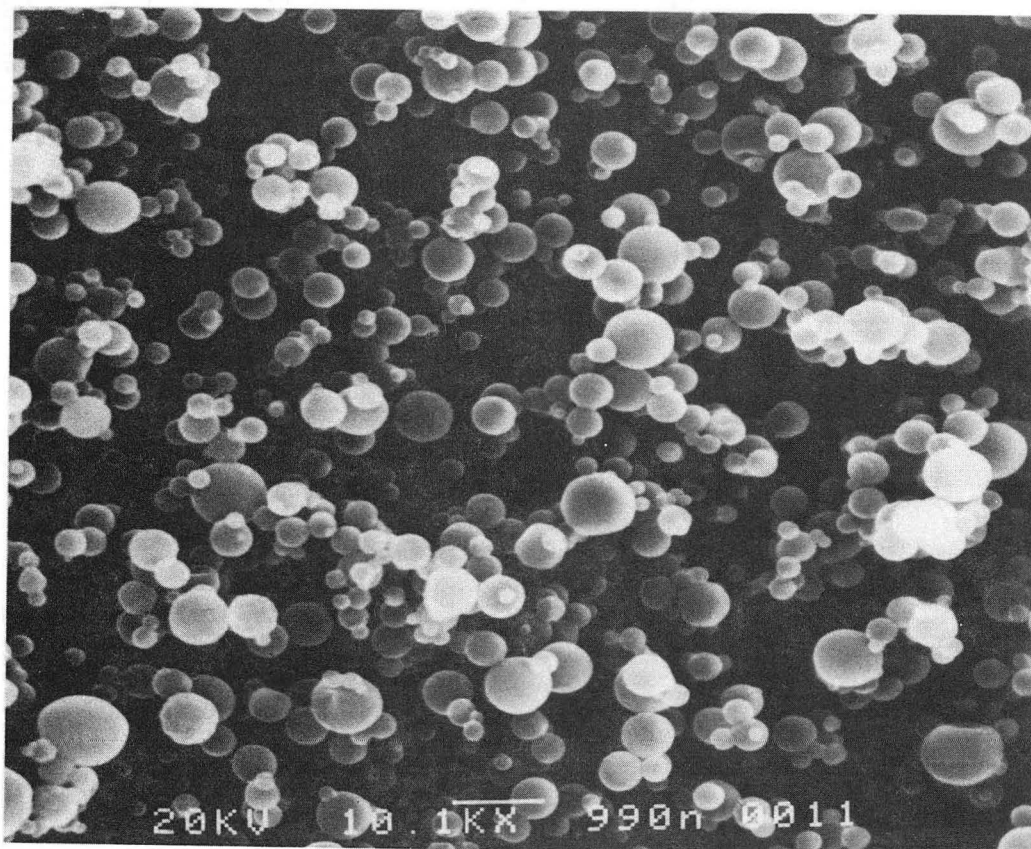
XBB 839-8198

Figure 10.   Scanning electron micrograph of cigarette smoke particles
micro-encapsulated and captured on a nuclepore filter.
The bar at the bottom of the photograph represents 0.99 μm.

```
┌─────────────────┐  ┌──────────────┐  ┌──────────────┐  ┌──────────────┐
│   CONTINUOUS    │  │   RADON      │  │   INDOOR     │  │  WEATHER:    │
│     RADON       │  │  DAUGHTER    │  │ ENVIRONMENT: │  │              │
│    MONITOR      │  │  CAROUSEL    │  │              │  │ Wind speed/  │
│   (CRM) - (4)   │  │              │  │Temperature(2)│  │ direction;   │
│                 │  │              │  │ Humidity (2) │  │ Temperature  │
└─────────────────┘  └──────────────┘  └──────────────┘  └──────────────┘
```

PRINTING TERMINAL

MAGNETIC TAPE

CRT TERMINAL

(Command/ status)

Data Retrieval

IAQ Research House Computer

Control

RADON INJECTION

MECHANICAL SYSTEMS:

Mixing fans; Ventilation; Furnace fan

PARTICULATE SYSTEMS:

Gas range operation; Control device operation

XBL 839-3235

Figure 11.   Block diagram of the Indoor Air Quality Research House
computer system.

SAMPLING LINES
from test space (6)
(1 cm diam; ~ 4 - 7 m long)

MANIFOLD

EM

OPTICAL PARTICLE
COUNTER

ELECTRO-
STATIC
CLASSIFIER

Sheath air in

Q = 15 cc/min

3-way
valve

CONDENSATION
NUCLEUS
COUNTER

Excess air flow
Q ~ 15 - 20 l/min

EM

M

Q = 300 cc/min

^{85}Kr NEUTRALIZER

Q ~ 1.7 - 4.7 l/min

M

Monodisperse
aerosol flow out
Q ~ 2 - 5 l/min

Q = 5 l/min

Key:

(M) Mass flow control

Diaphragm pump

⊗ Manual ball valve

EM Electro-mechanical ball valve

XBL 839-3239

Figure 12.   Schedule drawing of the particulate instrumentation and
sampling manifold of the Indoor Air Quality Research House.
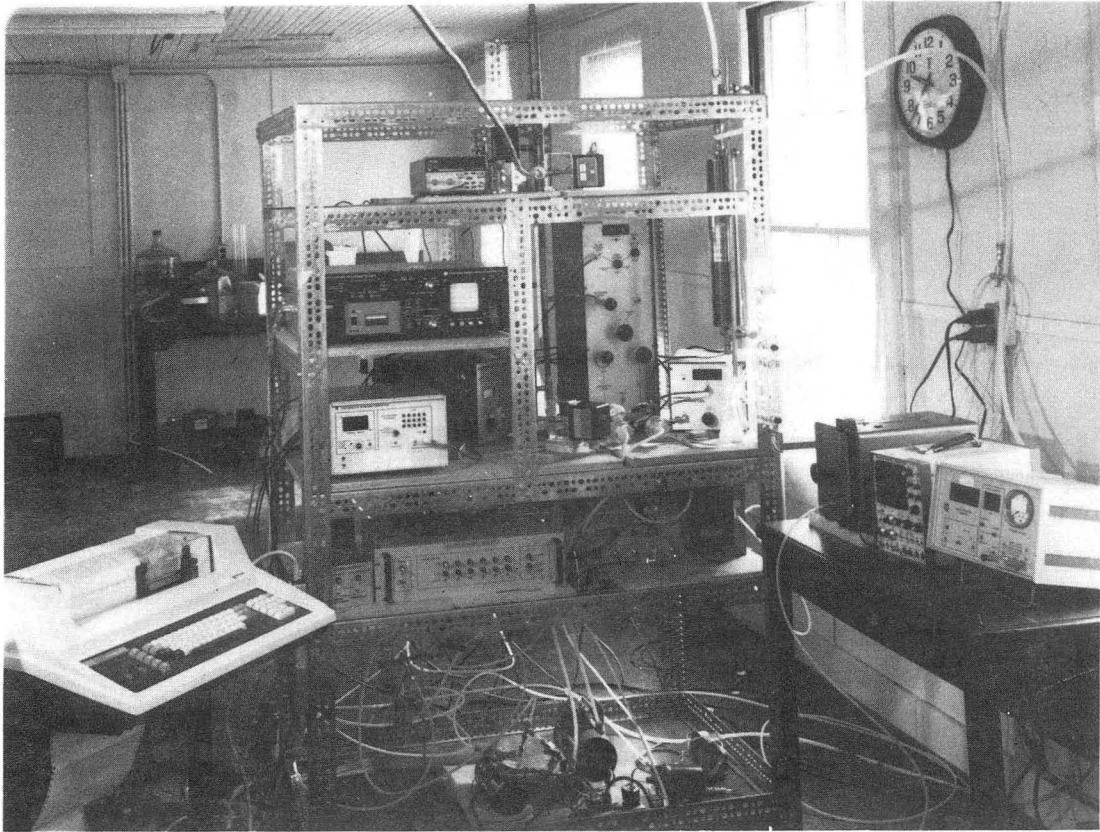
CBB 836-5362

Figure 13.   Photograph of the particulate instrumentation and sampling manifold at the Indoor Air Quality Research House.

CBB 836-5362

Figure 13.   Photograph of the particulate instrumentation and sampling manifold at the Indoor Air Quality Research House.
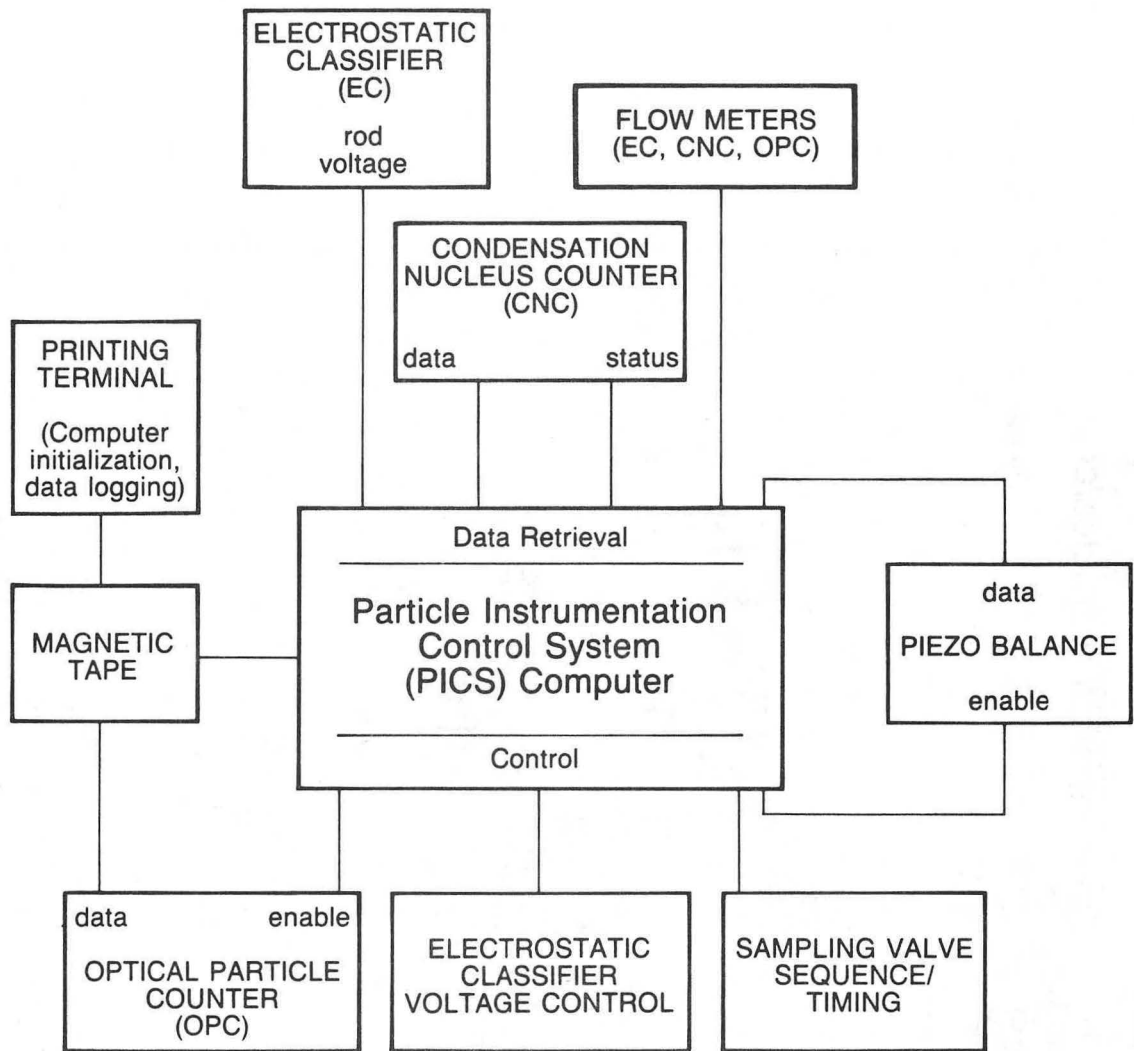
Figure 14.   Block diagram of the Particulate Instrumentation
              Control System.
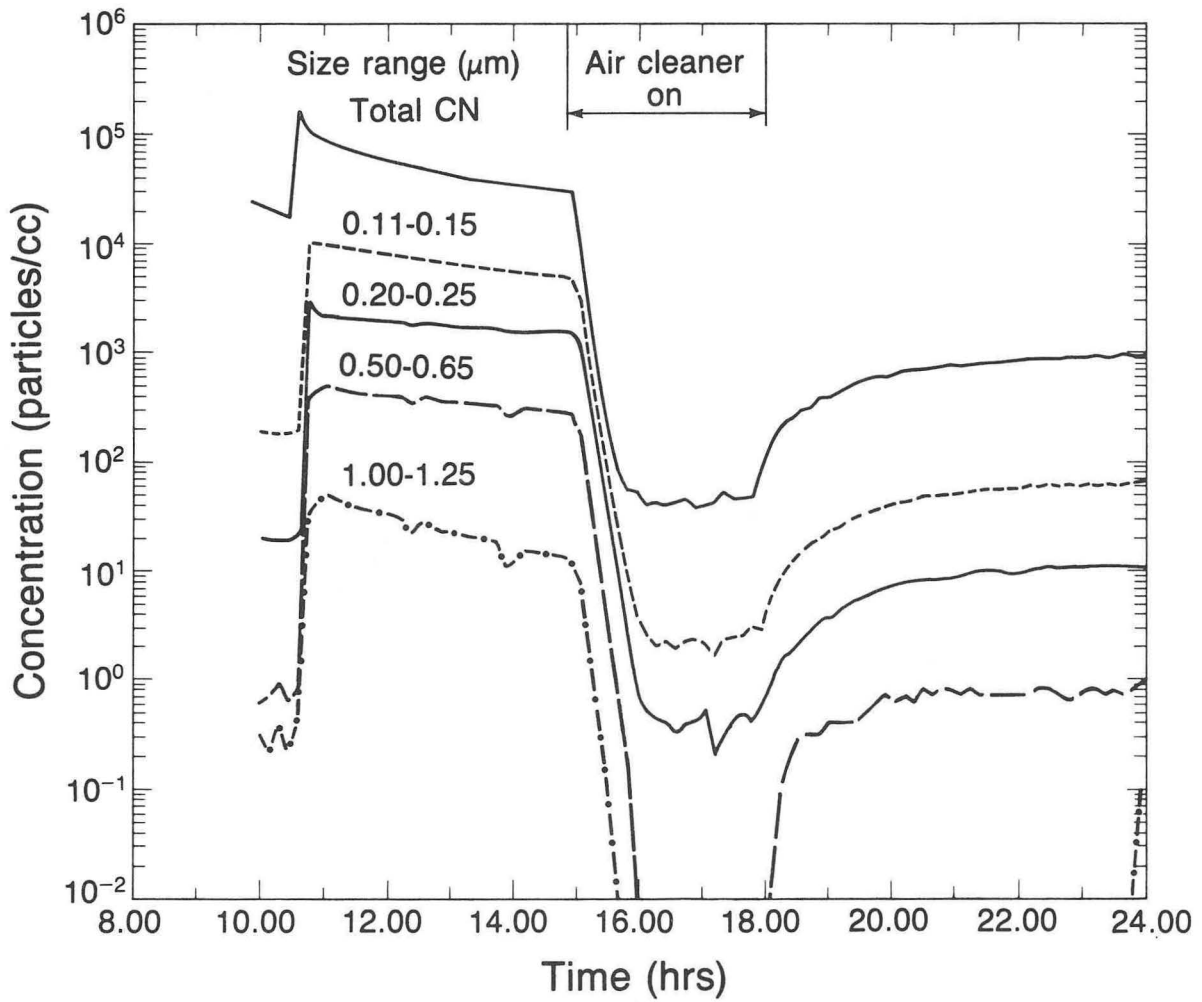
Figure 15.   Semi-log plot of particle concentration as a function of time for a single-room decay experiment using tobacco smoke and HEPA-type filter.
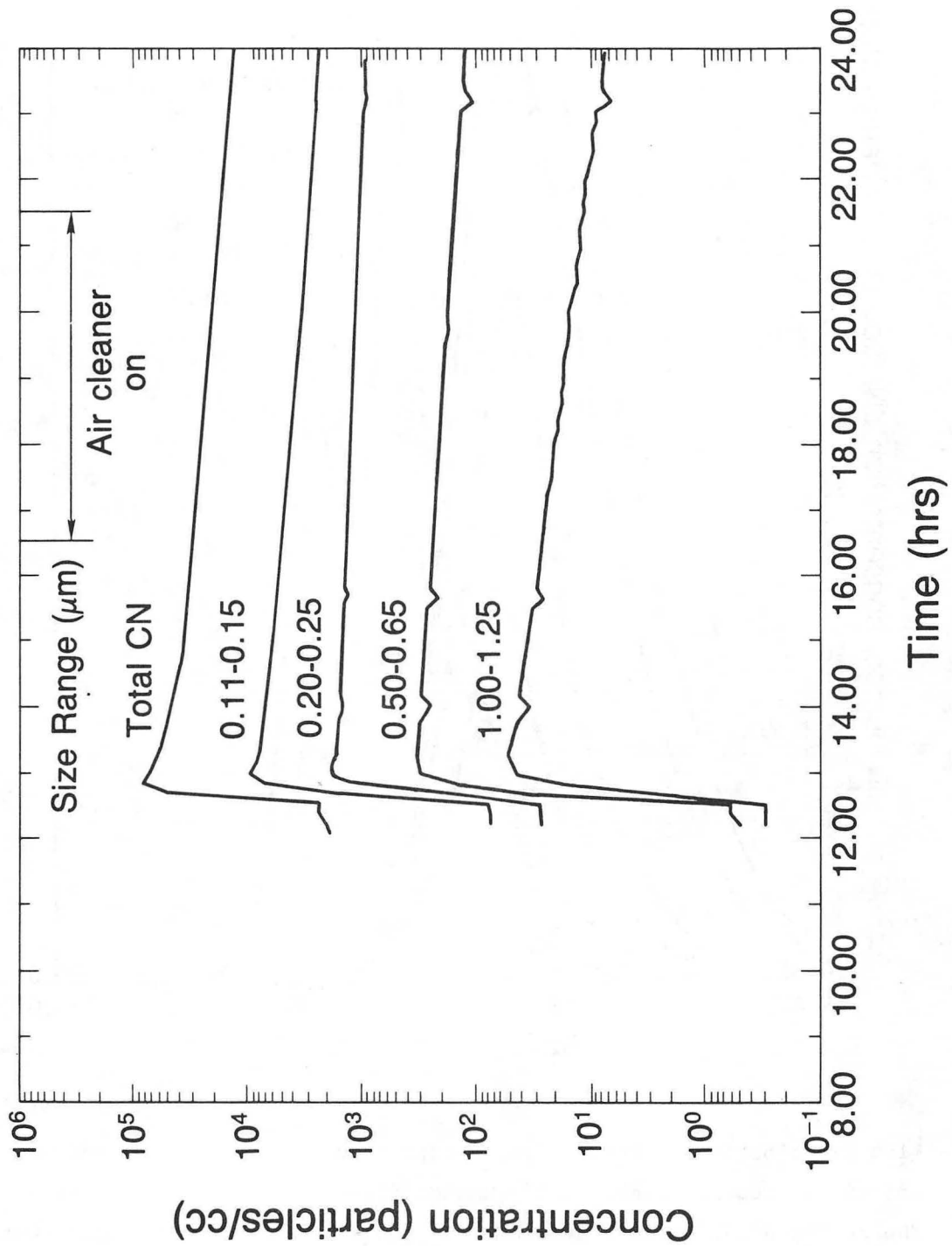
Figure 16.   Semi-log plot of particle concentration as a function of
time for a single-room decay experiment using tobacco smoke
and a small panel-filter air cleaner.
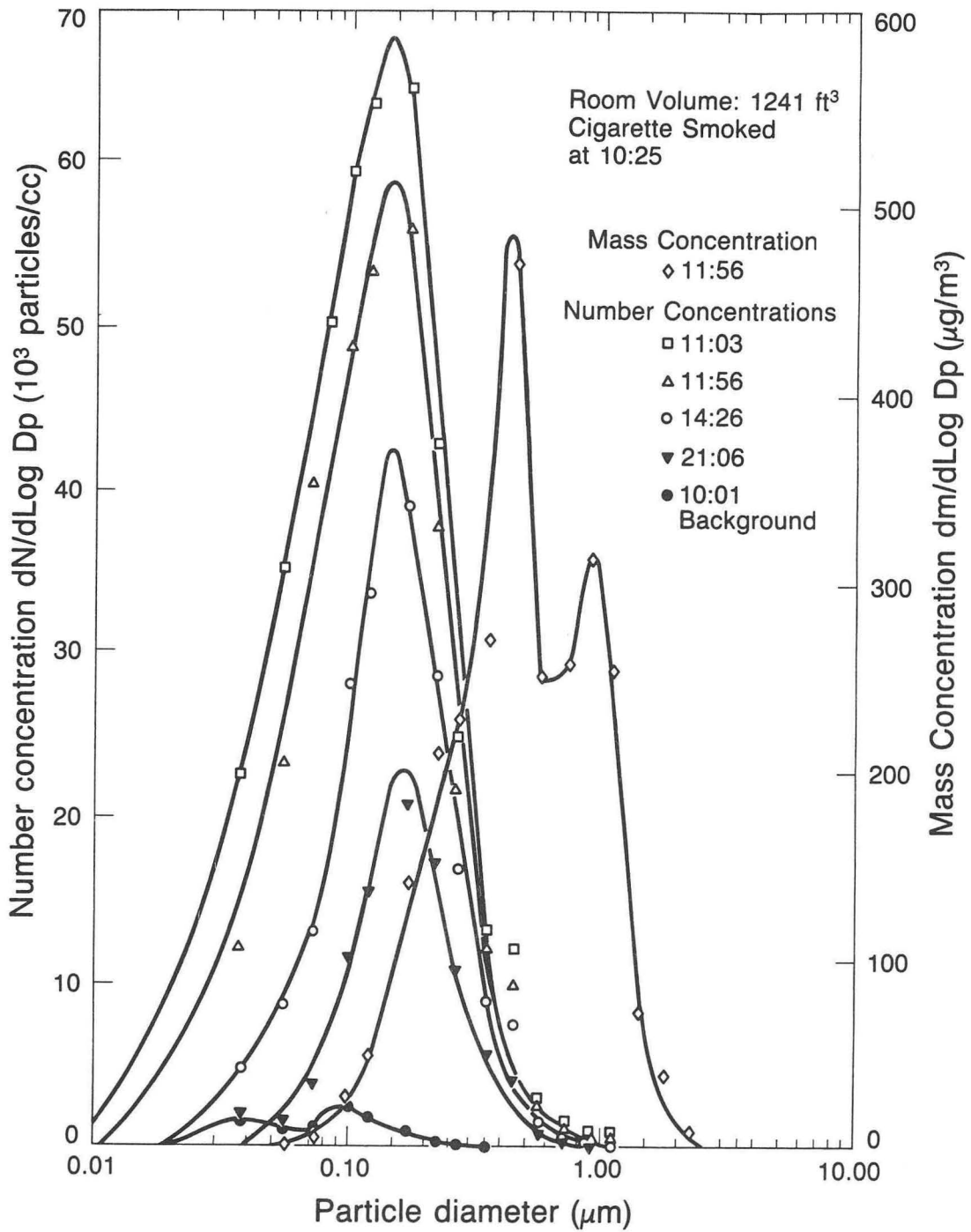
Figure 17.   Size distribution of tobacco smoke generated from mainstream and sidestream
emissions from one mechanically-smoked filtered cigarette in a 1200 ft^3 room.
The number distributions are based on concentration measurements, while the
mass distribution is derived from the number distribution at 11:56, assuming
spherical particles with a density of 1 gm/cm^3.

-86-
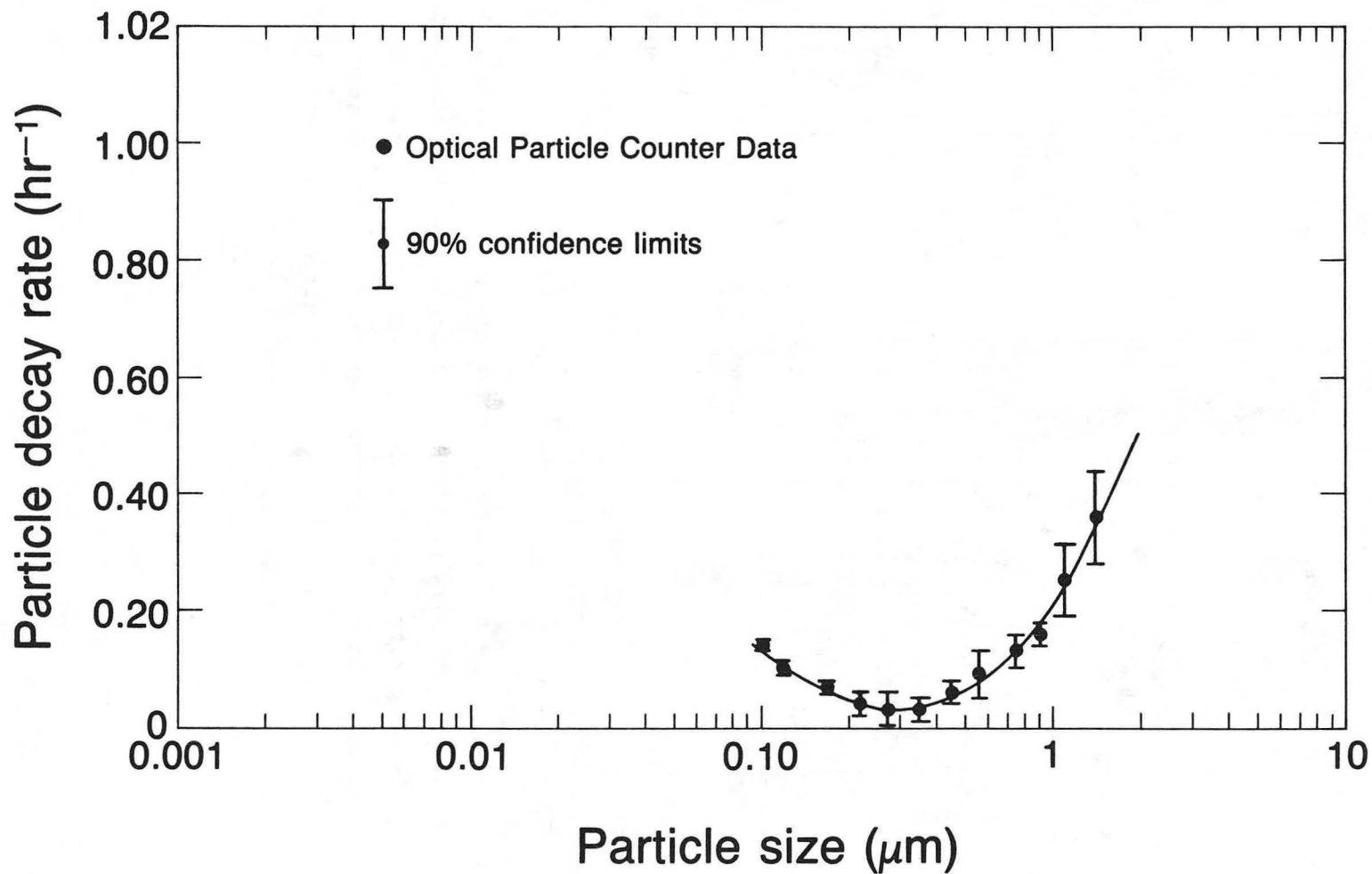
XBL 8310-3341

Figure 18.   Particle deposition rates as a function of particle size for
tobacco smoke, calculated as the observed particle decay
rate less the measured air-exchange rate.
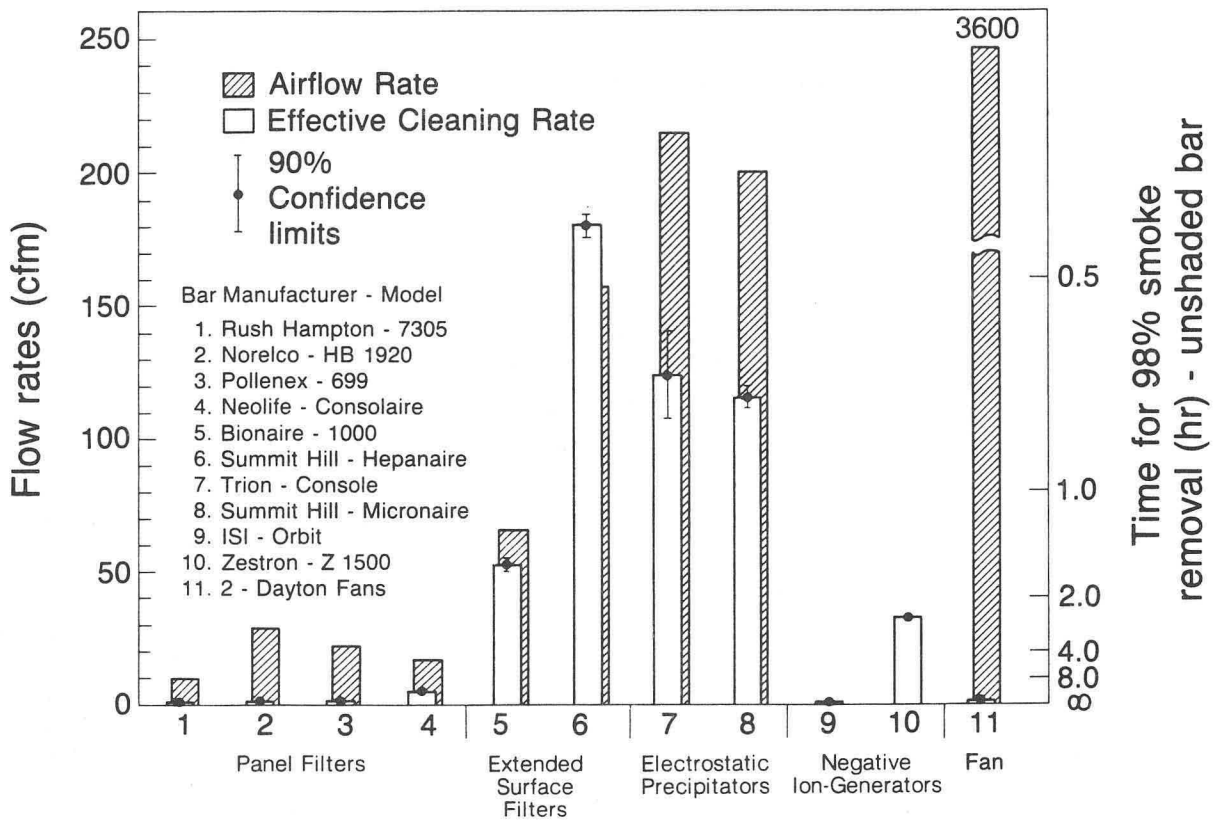
Figure 19.   Performance of various unducted air cleaning devices.
Shaded bar —airflow rates in cfm; unshaded bar - effective
cleaning rates in cfm; and time required for 98% smoke re-
moval in hours.   Effective cleaning rates calculated as the
flow rate of particle-free air required to produce the
observed decay rate of cigarette smoke.
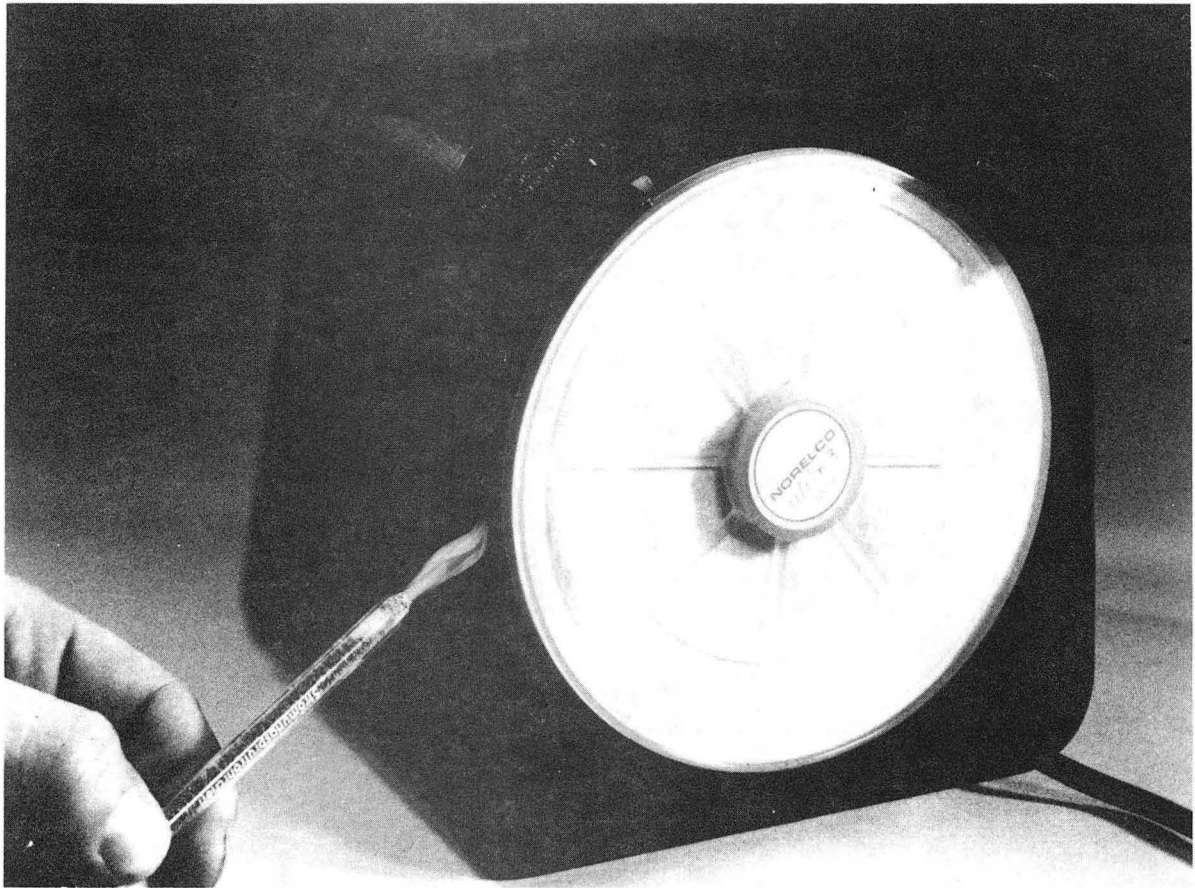
CBB 830-9823

Figure 20.   Airflow bypassing the filter element in an inexpensive
panel-filter air cleaner.

Other Removal
Processes:

Ventilation (λ_V) ⟵ **Radon** ○

Decay (λ_0)

Ventilation (λ_V) ⟵
————————————
Control Device (λ_F^f)

Unattached Progeny ● Plate-out (λ_{Po}^f) ⟶

Attachment
(X)

Recoil (^{218}Po only)
($r \lambda_1$)

Ventilation (λ_V) ⟵
————————————
Control Device (λ_F^a)

Attached Progeny ● Deposition (λ_d^a) ⟶

Particle

Wall or
Other
Macro
Surface
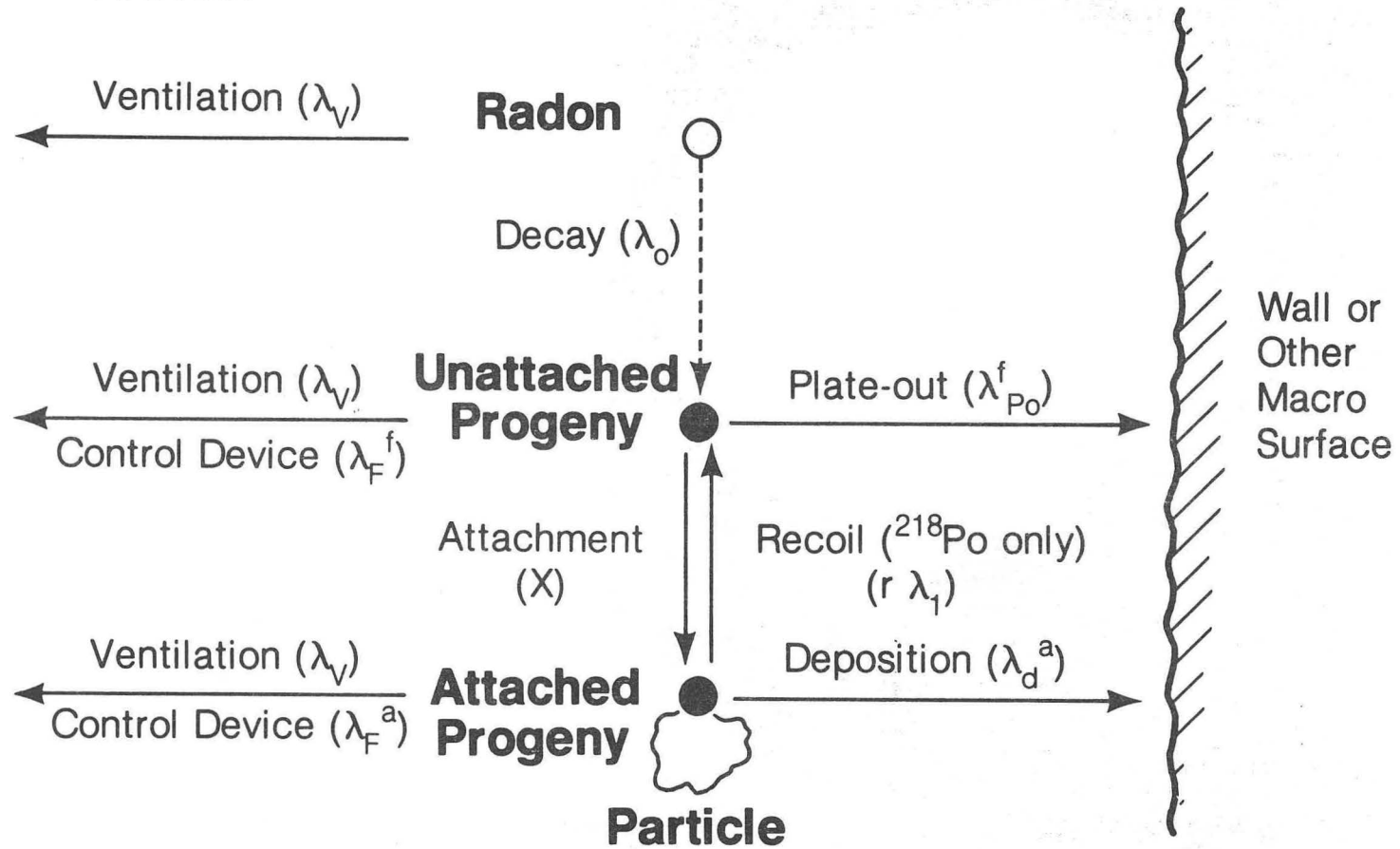
XBL 8311-647

Figure 21.   Schematic diagram of various decay and removal processes (and their associated rates) affecting concentrations of radon and radon progeny. The radioactive decay pathways for radon progeny are not explicitly noted in this diagram.
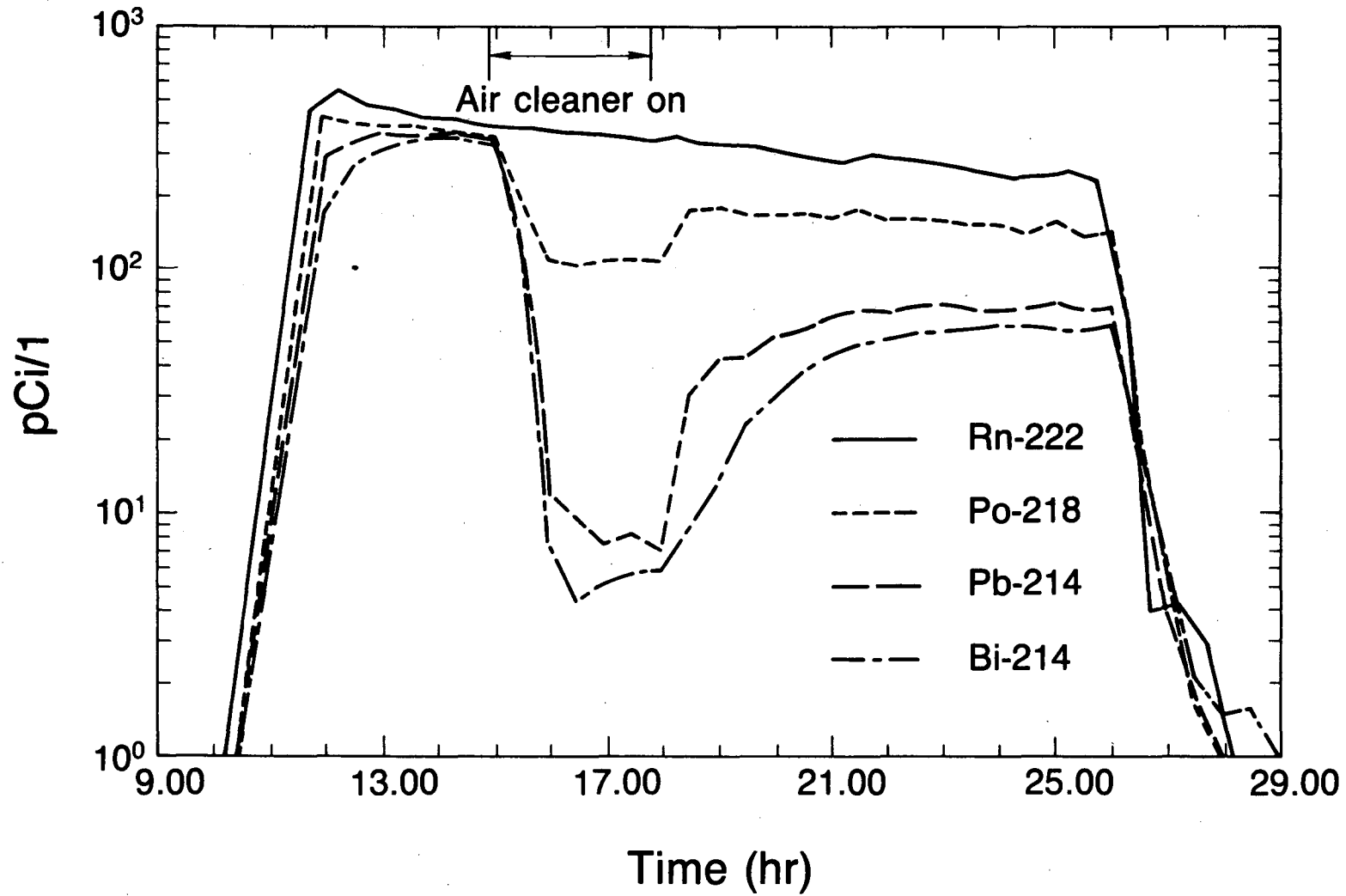
XBL 8312-6727

Figure 22. Semi-log plot of radon and radon progeny concentrations as a function of time, showing the effects of operation of a HEPA-type filter.
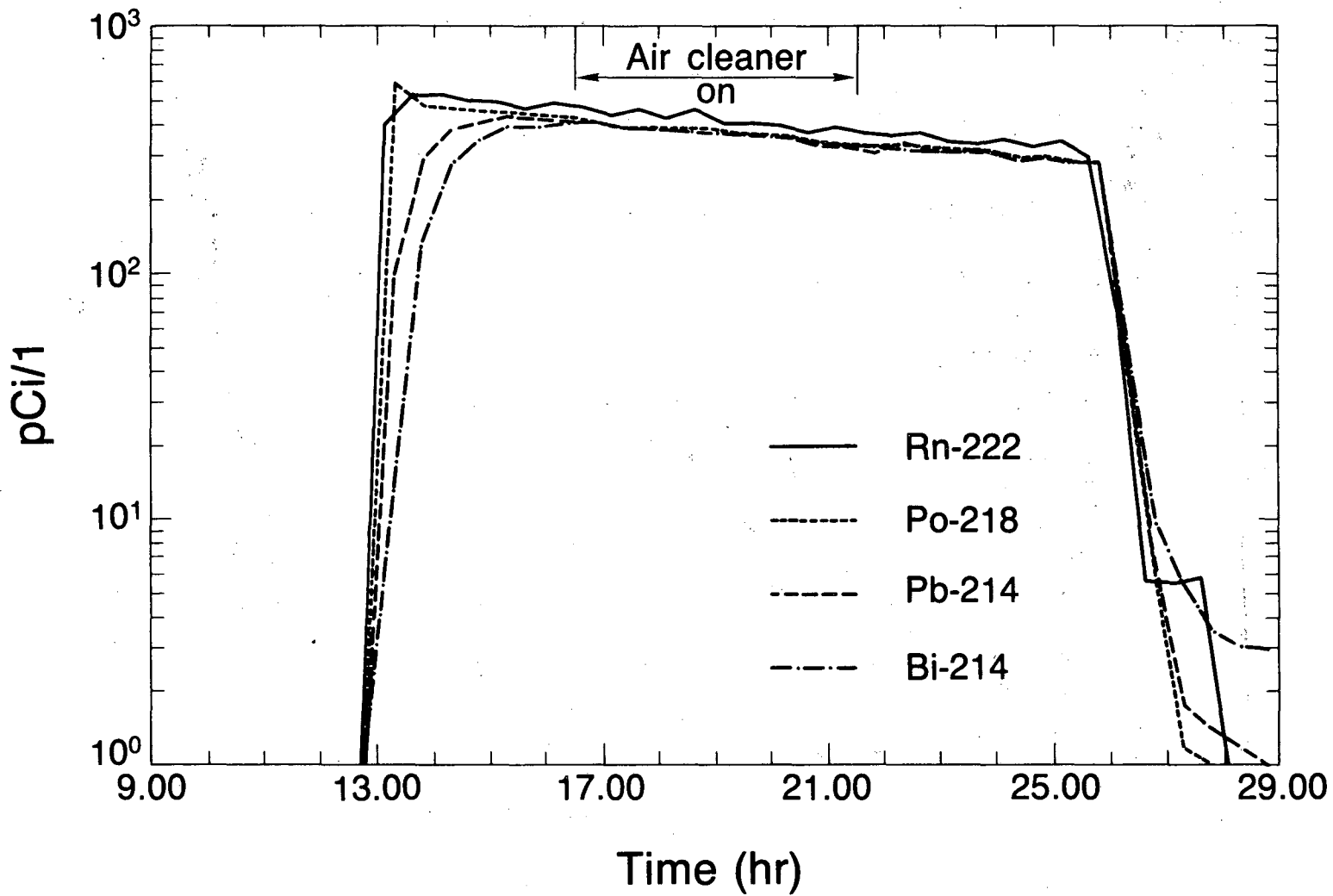
XBL 8312-6726

Figure 23.   Semi-log plot of radon and radon progeny concentrations as a function
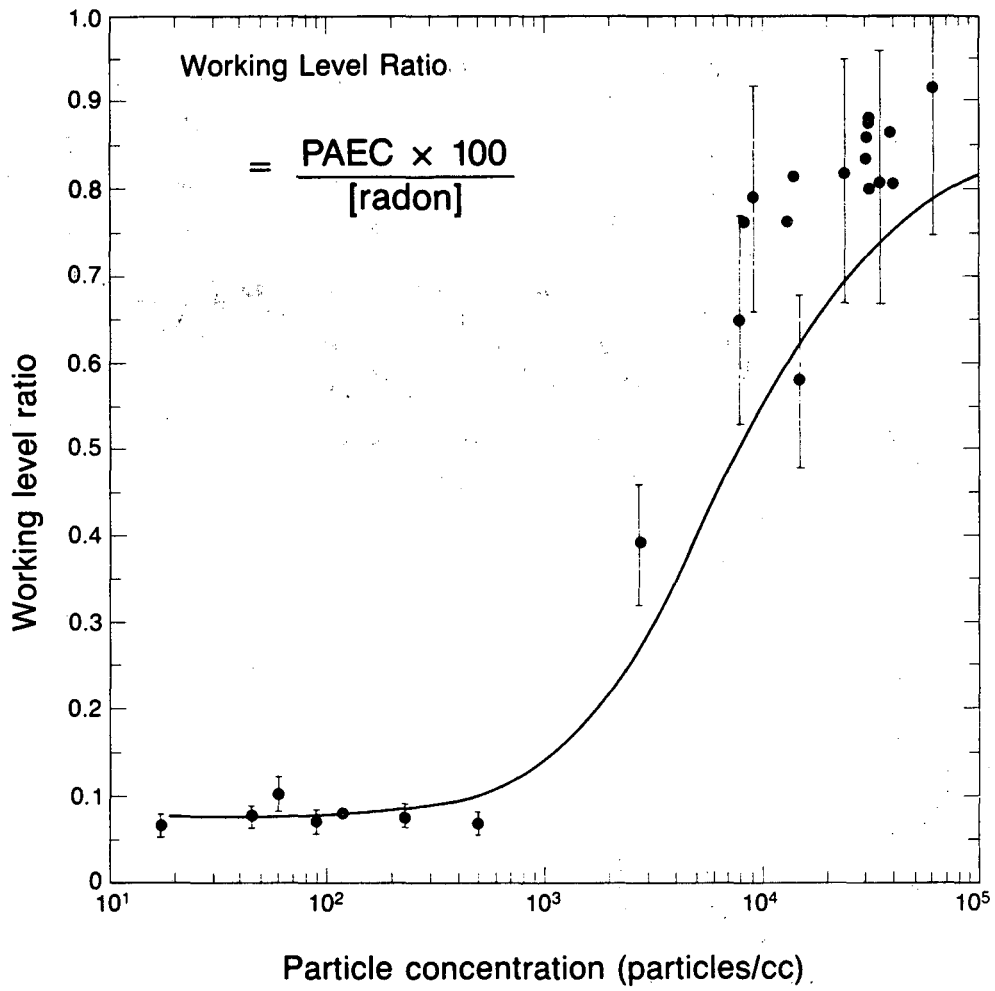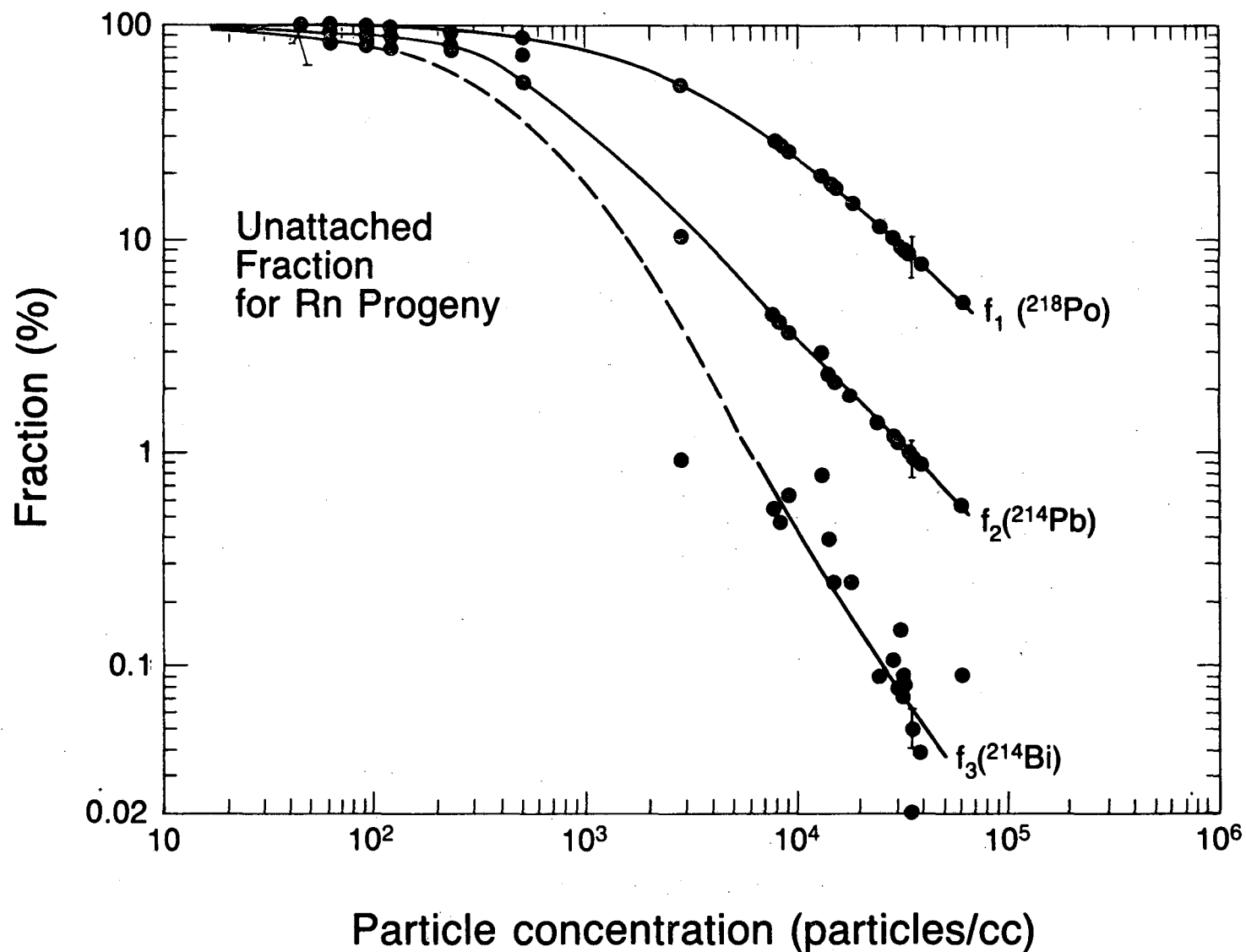of time, showing the effects of operation of a panel-filter device.

Figure 24.   Working Level Ratio versus particle concentration. Measured data
and representative uncertainties are shown as points and error
bars, while the solid line is based on calculated values.

Figure 25. Unattached fractions for radon progeny, ^{218}Po, ^{214}Pb, and ^{214}Bi, as a function of particle concentration. The lines through the data serve to guide the eye.

XBL 8312-6707

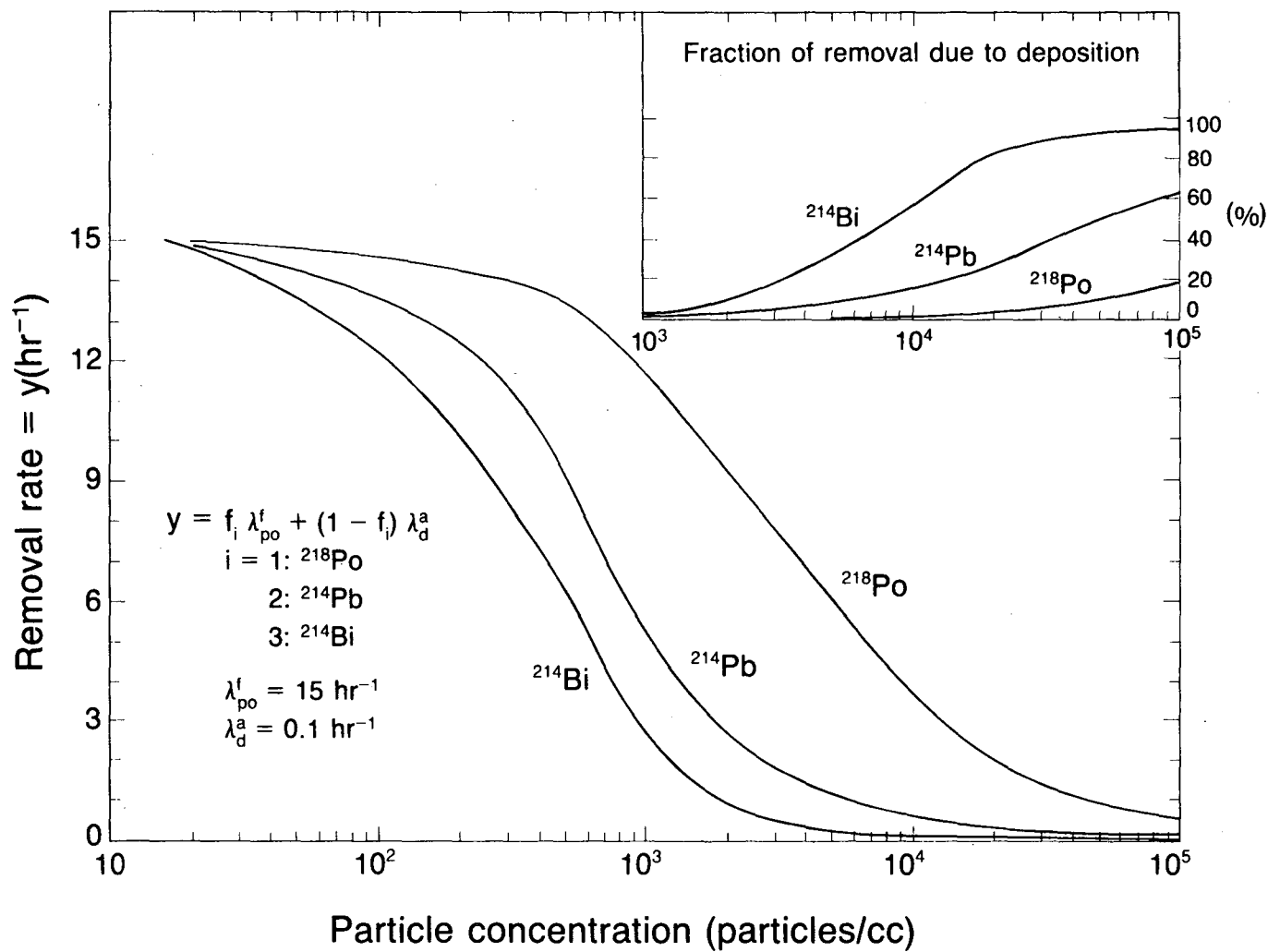Removal rate = y(hr^{-1})

Particle concentration (particles/cc)

Fraction of removal due to deposition

^{214}Bi

^{214}Pb

^{218}Po

(%)

$y = f_i \, \lambda_{po}^f + (1 - f_i) \, \lambda_d^a$
$i = 1$: ^{218}Po
$\quad 2$: ^{214}Pb
$\quad 3$: ^{214}Bi

$\lambda_{po}^f = 15 \text{ hr}^{-1}$
$\lambda_d^a = 0.1 \text{ hr}^{-1}$

^{218}Po

^{214}Bi

^{214}Pb

XBL 8312-6708

Figure 26.   Removal rate of airborne radon decay products due to plateout
of unattached progeny and deposition of progeny attached to
environmental aerosols.